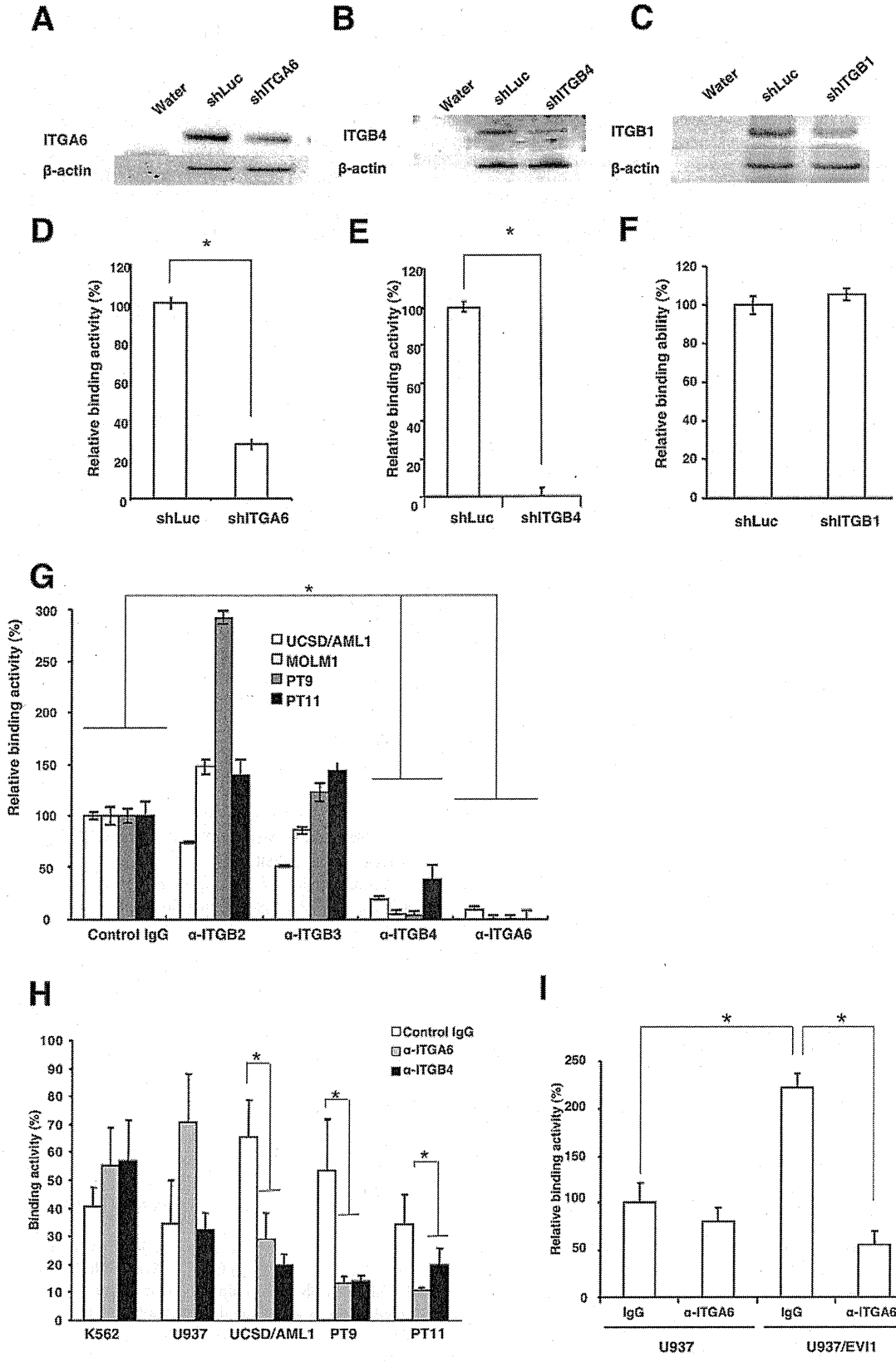
A
Water
shLuc
shITGA6
ITGA6
β-actin
B
Water
shLuc
shITGB4
ITGB4
β-actin
C
Water
shLuc
shITGB1
ITGB1
β-actin
D
Relative binding activity (%)
shLuc
shITGA6
E
Relative binding activity (%)
shLuc
shITGB4
F
Relative binding ability (%)
shLuc
shITGB1
G
Relative binding activity (%)
UCSD/AML1
MOLM1
PT9
PT11
Control IgG
α-ITGB2
α-ITGB3
α-ITGB4
α-ITGA6
H
Binding activity (%)
Control IgG
α-ITGA6
α-ITGB4
K562
U937
UCSD/AML1
PT9
PT11
I
Relative binding activity (%)
IgG
α-ITGA6
IgG
α-ITGA6
U937
U937/EVI1

Figure 3. The adhesion ability of EVI1^{high} leukemia is specifically dependent on the expression of ITGA6 and ITGB4. A, B, and C. UCSD/AML1 cells were transiently transfected with expression vectors for shRNA against ITGA6 (shITGA6), ITGB4 (shITGB4), or ITGB1 (shITGB1), and the expression of ITGA6, ITGB4 and ITGB1 was determined using RT-PCR. UCSD/AML1 cells transfected with shRNA for firefly luciferase (shLuc) were used as a control, and the expression of b-actin was used as an internal control. **D, E, and F.** The cell adhesion ability of the cells in A, B, and C was determined through co-culture with the MC3T3-E1 cell line. The relative binding activity was calculated by comparison to the basal binding activity of control AML1/shLuc cells. **G.** The effect of neutralizing antibodies to the integrins on the cell binding activity of EVI1^{high} leukemia cells. Two leukemia (UCSD/AML1 and MOLM1) and two primary human AML (PT9 and PT11) cell lines were cultured on matrigel-coated plates in the presence or absence of anti-ITGA6, ITGB2, ITGB3, or ITGB4 antibodies. The relative binding activity was calculated by comparison to the basal binding activity of each cell line treated with the control isotype IgG. **H.** Two EVI1^{low} (K562 and U937) and three EVI1^{high} (UCSD/AML1, PT9 and PT11) leukemia cell lines were treated with anti-ITGA6 or ITGB4 antibodies or with the control IgG, and the binding of each cell line to the matrigel-coated plates was determined. **I.** The parental and EVI1-expressing (U937/EVI1) U937 cell lines were treated with anti-ITGA6 or control IgG, and their binding to the MC3T3-E1 cell line was determined. The relative binding activity was calculated by comparison to the basal binding activity of the parental U937 cells treated with the control isotype IgG. Each experiment was performed in triplicate, and the experiments were independently repeated at least three times. The data are given as the mean ± S.E. The statistical analysis was performed using the Student's *t-test* (*$p<0.05$, vs. each control).
doi:10.1371/journal.pone.0030706.g003

significantly higher when the cells were cultured on matrigel-coated plates compared with conventional culture; however, the percentage of surviving AML1/shITGB4 cells was reduced at each time point.(**Fig. 5E**). The survival rate of the AML1/shEVI1 cells in both the conventional and matrigel-coated cultures was reduced compared with those of the AML1/shLuc and AML1/shITGB4 cells upon Ara-C treatment, whereas there was no difference in the survival rates of the AML1/shEVI1 cells cultured under conventional and matrigel-coated methods under Ara-C treatment. These results suggest that the drug resistance of EVI1^{high} leukemia cells is highly dependent on EVI1 expression and partially dependent on ITGB4 expression.

EVI1^{high} leukemia cells become more quiescent when cultured on the matrigel-coated plates compared with those cultured on the BSA-coated plates

To confirm the advantages of cell adhesion in drug-responsiveness, we determined the growth and cell cycle status of AML cells with EVI1$^{high/low}$, which were cultured on matrigel or BSA-coated plates. As shown in **Fig. 6A**, the UCSD/AML cells with EVI1^{high} expression (AML1/shLuc) on the matrigel-coated plates grew more faster rapidly on the matrigel-coated plates than that on the BSA-coated plates, although the growth rate of the AML1/shLuc cells was faster than that of the AML1/shEVI1 cells. The cell cycle analysis represented revealed that, relative to AML1/shLuc cells cultured on the BSA-coated plates, the population of EVI1^{high} AML1 cells in G0/G1 and G2/M phase increased on the matrigel-coated plates, while the S-phase populations were decreased; however, each cell cycle population of AML1/shEVI1 cells did not change under either culture condition (**Fig. 6B and C**). Moreover, the population of AML1/shLuc cells in the G0 phase was significantly increased on the matrigel-coated plates compared with the same cells on the BSA-coated plates; however, the population of AML1/shEVI1 cells in the G0 phase was the same under both culture conditions (**Fig. 6D**). Because the population of U937 cells with high EVI1 expression (U937/EVI1)

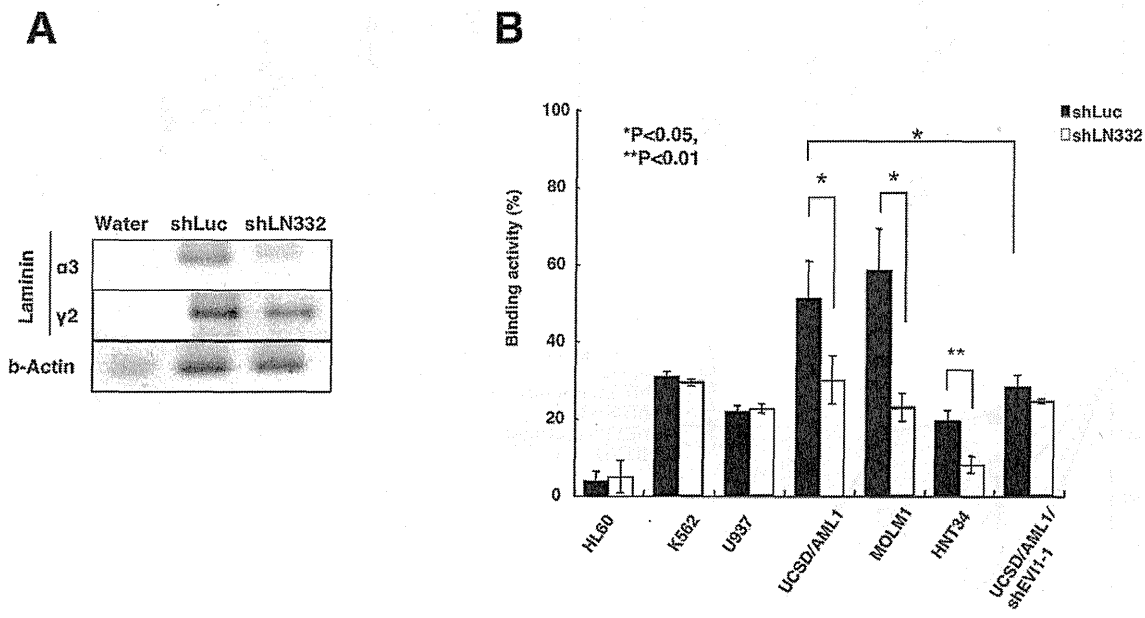

Figure 4. Laminin-332 on MC3T3-E1 cells is a main target for binding to EVI1^{high} leukemia cells. A. The expression of laminin a3 and g2 in MC3T3-E1 cells transfected with shRNA for firefly luciferase (shLuc) or laminin a3 (shLN332) was determined using RT-PCR. The expression of b-actin was used as an internal expression control. **B.** The binding of various myeloid leukemia cell lines to the two cell lines MC3T3-E1/shLuc or/shLN332 was determined. Each experiment was performed in triplicate, and the experiments were independently repeated at least three times. The data are given as the mean ± S.E. The statistical analysis was performed using the Student's *t-test* (**$p<0.01$; *$p<0.05$, vs. control).
doi:10.1371/journal.pone.0030706.g004

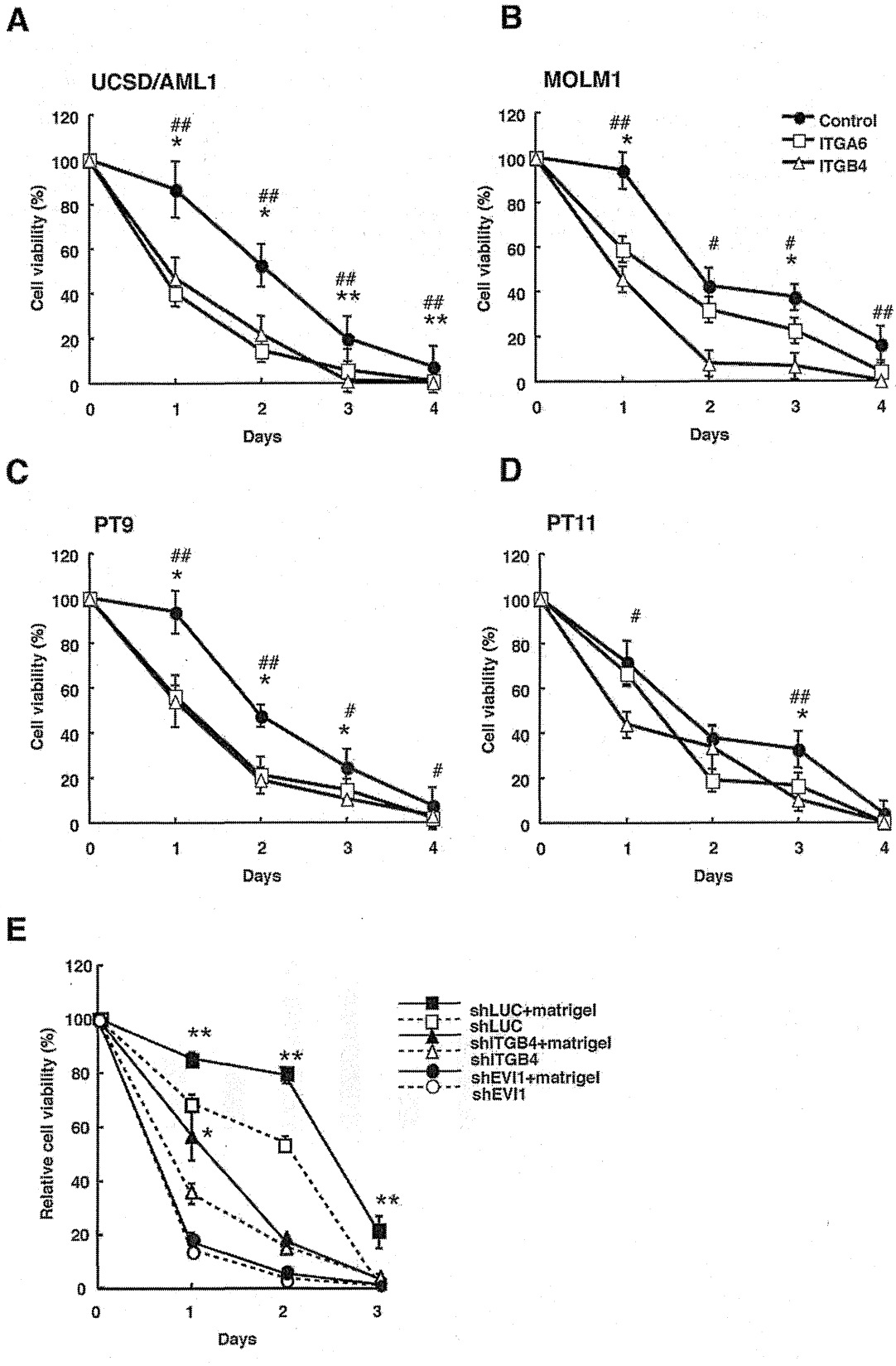
A
UCSD/AML1
Cell viability (%)
Days
B
MOLM1
Control
ITGA6
ITGB4
C
PT9
D
PT11
E
Relative cell viability (%)
shLUC+matrigel
shLUC
shITGB4+matrigel
shITGB4
shEVI1+matrigel
shEVI1

Figure 5. Drug sensitivity of EVI1^{high} leukemia cells is restored by treatment with neutralizing antibodies to ITGA6 or ITGB4 or by transfection with small hairpin RNAs against EVI1 or ITGB4. A–D. Two myeloid leukemia (UCSD/AML1 and MOLM1) and two primary AML (PT9 and PT11) cell lines were treated with 1×10^{-6} M Ara-C and anti-ITGA6 or ITGB4 antibodies for four days, and the viable cells were counted at each indicated time point. The percent cell viability in comparison with the number of untreated cells on each indicated day is shown. **E.** The UCSD/AML1 cells expressing shRNA for firefly luciferase (shLuc), ITGB4 (shITGB4) or EVI1 (shEVI1) were treated with Ara-C on BSA or matrigel-coated plates for three days. The viable cells were counted at each time point. The relative cell viability is expressed as a percentage of the viability of the untreated cells. Each experiment was performed in triplicate, and the experiments were independently repeated at least three times. The results are given as the mean ± S.E. The statistical analysis was performed using the Student's *t-test* (**$p<0.05$, vs. control).
doi:10.1371/journal.pone.0030706.g005

in the G0-phase was increased on the matrigel-coated plates compared with those on the BSA-coated plates (**Fig. S5**), the increased quiescence of adhered EVI1^{high} AML cells might be one of the reasons for resistance to anti-cancer drugs.

Discussion

Resistance to treatment with anti-cancer drugs is determined by a variety of factors, including somatic cell genetic differences in tumors and the phenotypes of leukemia stem cells (LSC). LSCs can infiltrate bone marrow niches, leading to enhanced self-renewal and proliferation, and enforced quiescence; the resistance to chemotherapeutic agents and adhesion molecules, such as VCAM-1 and VLA-4, has been described in the localization and retention of normal HSCs and/or leukemia cells within the bone marrow niche [19]. In this manuscript, we examined the cell adhesion ability of EVI1^{high} leukemia cells because the increased expression of EVI1 in AML is a well-known prognostic factor for poor outcome and is associated with drug resistance [4,5]. We found that the EVI1^{high} leukemia cells with increased ITGA6 and ITGB4 expression exhibited stronger adhesion to laminin complexes than the EVI1^{low} leukemia cells; although, the EVI1^{low} leukemia cells exhibited increased adhesion to fibronectin. Moreover, the interaction between EVI1^{high} leukemia and MC3T3-E1 osteoblastic cells was partially dependent on laminin-332. The downregulation of EVI1 or ITGB4 in UCSD/AML1 leukemia cells restored chemo-sensitivity. The knockdown of ITGA6 expression in EVI1^{high} leukemia cells greatly reduced their survival in culture; thus, we conclude that the increased cell adhesion ability of EVI1^{high} leukemia cells is primarily dependent on the expression of ITGA6, and that signaling from IGTA6 is crucial for the survival of EVI1^{high} leukemia cells.

The expression of the ITGA6/ITGB4 complex could promote tumor progression and the metastasis of various cancer cells, including breast, colorectal, and thyroid carcinomas. Moreover, the laminin receptor for ITGA6 is ubiquitously expressed in human and mouse hematopoietic stem and progenitor cells [26]. In combination with ITGA4, ITGA6 expression in hematopoietic stem and progenitor cells is believed to create a homing receptor for short-term stem cells [27]. ITGA6 functions during the homing of fetal liver HPCs but not during the homing and engraftment of multilineage repopulating HSCs *in vivo* [28]. Therefore, ITGA6 might function as a laminin receptor to sustain HSCs in the bone marrow niche. We are now developing anti-human ITGA6/ITGB4 complex antibodies, which is a new therapy for refractory AML. In preliminary experiments, we demonstrated that the number of EVI1^{high} AML cells was significantly decreased in the bone marrow after the intravenous injection of anti-human ITGA6/ITGB4 complex antibodies into NOG immune deficient mice (data not shown). As a corollary, the increased expression of the ITGA6/ITGB4 complex in EVI1^{high} leukemia might be an important factor in maintaining leukemia stem cells in the bone marrow.

The adhesion of EVI1^{high} AML cells became more resistance to anti-cancer drug therapy, and the population of cells in the G0-phase was increased. Because the increased population of G0-phase cells is likely dependent on the expression of EVI1, future research should focus on the characterization of the mechanism underlying the increased quiescent of cells through EVI1 expression subsequent to their adhesion to matrigel. Moreover, the induction of PI-3K/AKT/Bcl-2 signaling through the VLA-4-fibronectin interaction results in resistance to anoikis and drug-induced apoptosis [21]; we also showed the cell adhesion of EVI1^{high} AML cells to matrigel induced expression of BCL and phosphorylation of AKT (data not shown). Therefore, the adhesion of AML cells may provide advantages to the surviving cells, and the mechanism of drug-resistance is potentially much more complicated; however, we should characterize the survival mechanism of leukemia cells in the bone marrow niche.

To support our data, we examined the expression patterns of ITGA6/ITGB4 and VLA-4 (ITGA4/ITGB1) heterodimers by comparing the gene expression profiles of EVI1^{high} and EVI1^{low} AML deposited in Gene Expression Omnibus (GSE6891, GEO in NCBI website) [29]. As shown in **Fig. S6**, the expression of ITGA6 was significantly higher in the 12 cases of EVI1^{high} AML than in the 10 cases of EVI1^{low} AML ($p<0.05$); however, the differences in expression of ITGB4, ITGA4 and ITGB1 did not account for the differences between the two groups. We also determined the expression patterns of four integrin genes from the expression profiles of AML cases in remission and relapse that were deposited in GEO at NCBI (GDS1059) [30]. Based on the expression profiles, the expression of ITGA6 was significantly higher in the 28 cases of AML with relapse than in the 25 cases with remission ($p<0.05$); however, the differences in expression of ITGB4, ITGA4 and ITGB1 did not account for the difference between the two groups. These results show that the increased expression of ITGA6 is an important marker in both EVI1^{high} and relapsed AML, which suggests that ITGA6 might be an important target for the molecular-targeted treatment of refractory leukemia, including EVI1^{high} AML.

Materials and Methods

Cell lines and culture conditions

The MOLM1, HNT34, U937, K562, and HL60 cells were cultured in RPMI1640 medium supplemented with 10% fetal calf serum at 37°C and 5% CO_2. The UCSD/AML1, PT9 and PT11 cells [24] were cultured in RPMI1640 medium supplemented with 10% fetal calf serum and human granulocyte-macrophage colony stimulating factor (GM-CSF, 1 ng/ml) at 37°C and 5% CO_2. The MOLM1 cells were purchased from the Hayashibara Institute, and the MC3T3-E1 and HNT34 cells were purchased from the RIKEN cell bank. The 293T cells were cultured in high-glucose DMEM supplemented with 10% fetal calf serum, and the MC3T3-E1 cells were cultured in MEM alpha supplemented with 10% fetal calf serum.

Oligonucleotide microarray

This experimental method was previously described [24].

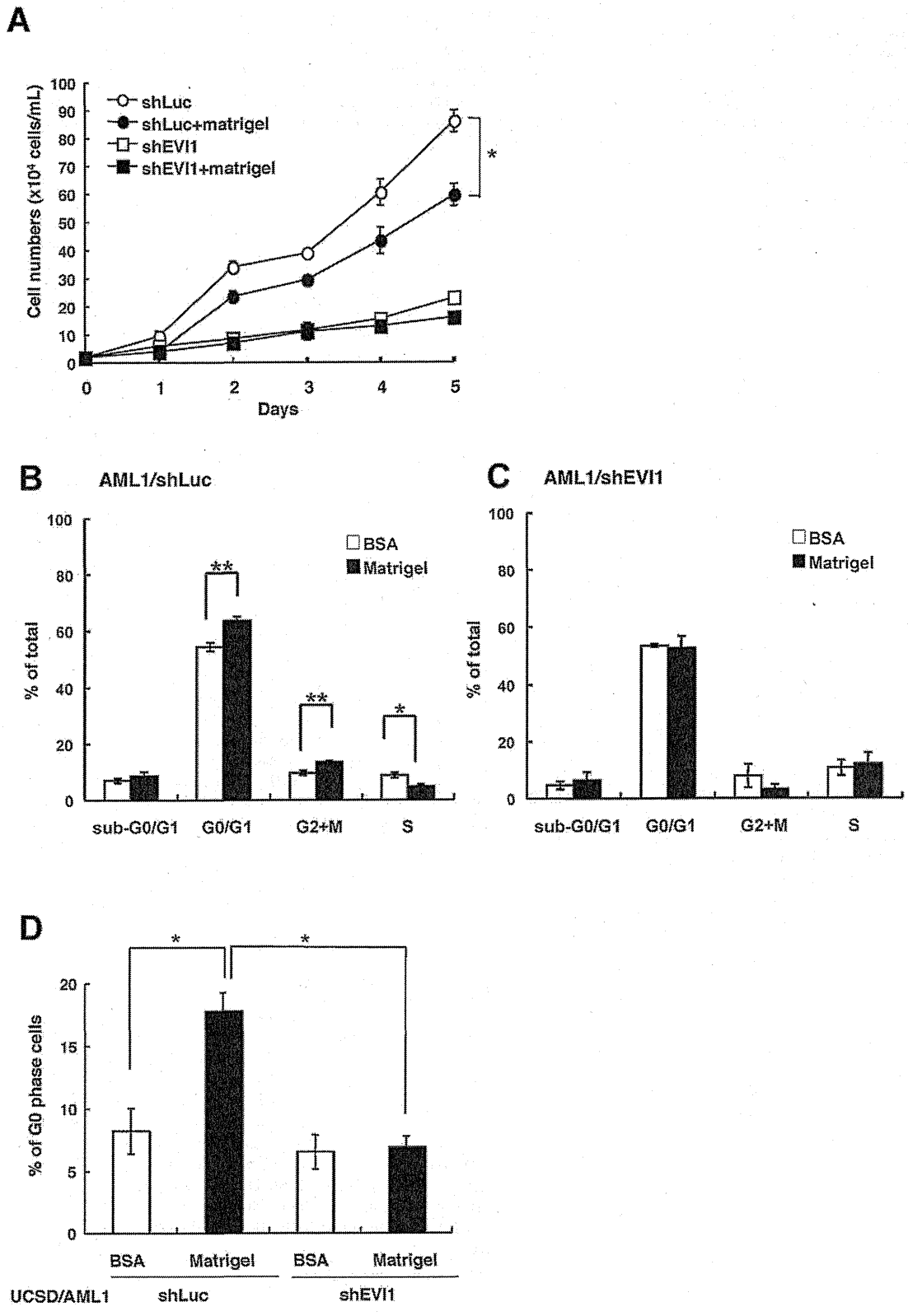
A
Cell numbers (x10⁴ cells/mL)
shLuc
shLuc+matrigel
shEVI1
shEVI1+matrigel
Days
B
AML1/shLuc
% of total
BSA
Matrigel
sub-G0/G1
G0/G1
G2+M
S
C
AML1/shEVI1
D
% of G0 phase cells
UCSD/AML1
shLuc
shEVI1

Figure 6. Decreased cell growth with increased cell population in G0-phase of EVI1^{high} AML cells cultured on the matrigel-coated plates. A. The UCSD/AML1 cells were transfected with shEVI1 (AML1/shEVI1) or control shLuc vector (AML1/shLuc) to determine their cell growth under normal culture conditions on BSA or matrigel-coated plates. **B and C.** The cell cycle of AML1/shLuc as a control (**B**) and AML1/shEVI1 (**C**) were analyzed using BD FACSCalibur after double staining with BrdU-APC and 7-AAD. The percentage of viable cells in each cell cycle is indicated with white (BSA-coated) and black (matrigel-coated) bars. **D.** The percentage of AML1/shEVI1 (black bars) and AML1/shLuc (white bars) cells in the G0 phase cultured on matrigel or BSA-coated plates were analyzed using BD FACSCalibur after double staining with Ki67-Alexa647 and 7-AAD. Each experiment was performed in triplicate, and the experiments were independently repeated at least three times. The results are shown as the mean ± S.E. The statistical analysis was performed using the Student's *t-test* (**$p<0.01$; *$p<0.05$, vs. control).
doi:10.1371/journal.pone.0030706.g006

Adhesion-mediated drug resistance (CAM-DR) in AML cell lines

The UCSD/AML1, MOLM1, PT9 and PT11 cells were plated onto tissue culture plates with BSA or matrigel-coated wells and subsequently incubated with 10^{-3} to 10^{-7} M cytosine-arabinoside (Ara-C) for 48 h. The number of viable cells was determined using trypan blue exclusion.

Neutralizing Antibody

The neutralizing antibodies used included rat anti-ITGA6 (Santa Cruz) and mouse anti-ITGB2, ITGB3 and ITGB4 (Millipore).

PCR and PCR primers

Total cellular RNA was isolated using Trizol (Invitrogen), and the cDNA was prepared using oligo(dT) primer and reverse transcriptase (SuperScript; Invitrogen). The polymerase chain reaction (PCR) was performed using Ex Taq (Takara-Bio) on a GeneAmp 2400 machine (Applied Biosystems). The primers for all integrin family members, EVI1 and b-actin were produced based on methods used in previous studies [12], [31]. The primers for N and VE-cadherin were produced based on the Quantitative PCR Primer Database (http://lpgws.nci.nih.gov/cgi-bin/PrimerViewer). The primers for the laminin family genes were produced based on Primer Bank (http://pga.mgh.harvard.edu/primerbank/).

Introduction of small hairpin RNAs for EVI1, ITGA6, ITGB1 and ITGB4 in UCSD/AML1 cells

The pSIREN-retroQ-ZsGreen plasmid (Takara-Bio) was used to inhibit EVI1 expression, and expression of ZsGreen (green fluorescent protein) was used as a marker. The following sequences were cloned into the BamHI-EcoRI sites of the pSIREN-retroQ-ZsGreen plasmid to create shRNAs against human EVI1 [32], 5′-GATCGCTCTAAGGCTGAACTAGCAGTTCAAGAGACT-GCTAGTTCAGCCTTAGATTTTTTG-3′; human ITGA6, 5′-GATCTCCTTTCAGGTTCAGTAGTTATTTCAAGAGAA-TAGTTACTGAATCTGAGAGGTTTTTG-3′; human ITGB1, 5′-GATCTGGAGGGTTGTTTCGGGTTTCATTCAAGAGA-TGAAGTCCGAAGTAATCCTCCTTTTTG -3′; and human ITGB4, 5′-GATCGCCAGCGACTACACTATTGGATCTCG-AGATCCAATAGTGTAGTCGCTGGTTTTTG (MISSION shRNA library, Sigma). We used the pSIREN-retroQ-ZsGreen-shLuc plasmid containing an shRNA against firefly luciferase (Takara-Bio) as a control. The retroviral particles were generated using the p10A1 packaging vector (Takara-Bio) via the transient transfection of 293T cells. The transfection was conducted using Hilymax liposome transfection reagent (Dojin). For retroviral transduction, 1×10^6 cells were plated onto a 6-cm dish containing 5 ml retroviral supernatant containing 100 ng/ml of polybrene for 24 h. After two weeks, the ZsGreen-positive cells were sorted using a JSAN cell sorter (Bay Bioscience). The reduction of EVI1 or ITGB4 expression was confirmed using RT-PCR.

Establishment of stable U937 cell lines expressing EVI1

The pGCDNsam-EVI1-IRES-EGFP construct was kindly provided by Dr. A. Iwama (Chiba University, Chiba, Japan). To produce recombinant retrovirus, the plasmid DNA was transfected into 293GP cells along with the vesicular stomatitis virus G (VSV-G) expression plasmid via $CaPO_4$ precipitation. For retroviral transduction, 1×10^5 U937 cells were plated onto 96-well flat-bottomed plates and infected for 24 h with either an EVI1 retroviral supernatant (pGCDNsam-EVI1-IRES-EGFP) or a control retroviral supernatant (pGCDNsam-IRES-EGFP) containing 100 ng/ml of polybrene. After 7 days, the green fluorescent protein (GFP)-positive U937 cells were sorted using a JSAN cell sorter (Bay Bioscience, Kobe, Japan).

Laminin-332 (laminin-5) knockdown in MC3T3-E1 cells

The pSIREN-retroQ-ZsGreen plasmid (Takara-Bio) was used to inhibit the expression of the a3 chain of laminin-332, and the expression of ZsGreen (GFP) was used as a marker. The following sequence was cloned into the BamHI-EcoRI sites of the plasmid to create an shRNA against the a3 chain of murine laminin-332: 5′-GATCTGAACTCCTTAAATGATTATGAATTCAAGAG-ATTCATAATCATTTAAGGAGTCTTTTTTTACGCGTG-3′. The target sequence for the knockdown was determined using the BLOCK-iT RNAi Designer (http://www.invitrogen.com/rnai). We used pSIREN-retroQ-ZsGreen-shLuc containing shRNA against firefly luciferase (Takara-Bio) as a control. We transiently introduced the laminin-332 or luciferase shRNA expression vector into MC3T3-E1 cells using an Amaxa Nucleofector (Lonza) and determined the expression levels of the a3 and g2 subunits of laminin-332.

Cell proliferation and cell viability assays

A cell proliferation assay was performed using a Cell Counting Kit-8 (Dojin) according to the manufacturer's protocol. Briefly, 5×10^3 cells/well were plated onto a 96-well culture plate and incubated for 1–3 days. Approximately 10 ml of Cell Counting Kit-8 reagent was added to the plate, and the absorbance at 450 and 620 nm was measured using an Immunomini NJ2300 plate reader (Nunc). A cell viability assay was performed using the Cell Counting Kit-8 reagent according to the manufacturer's protocol. For this assay, 5×10^3 cells were plated onto a 96-well culture plate containing Ara-C (1×10^{-6} M), rat anti-ITGA6 (20 mg/ml) or mouse anti-ITGB4 (20 mg/ml). The cells were incubated for 1–2 days and 10 ml of Cell Counting kit-8 reagent was added. The absorbance at 450 and 620 nm was measured. The cell viability was calculated by dividing the value obtained for the treatment well by the average value obtained for the control wells. For cell viability assay, cells were seeded in 5×10^4 cells/ml to matrigel coated culture plate. Cells were co-cultured with Ara-C (1×10^{-6} M) and anti-ITGA6 antibody (20 mg/ml) or anti-ITGB4 (20 mg/ml) or isotype control IgG (20 mg/ml). After incubation for 1 to 4 days, living cell numbers were counted by trypan blue exclusion. The cell viability was calculated by dividing the value for the treatment well by the value for the control wells. Each

experiment was performed in triplicate. Data are shown as mean ± S.E. Statistical analysis was performed using Student's *t-test.*

Cell adhesion assay

Four types of extracellular matrices (ECM; matrigel, fibronectin, laminin, collagen) and BSA (as a control) were used for the cell adhesion assay. A culture plate was coated overnight with a 1/40 dilution of Growth Factor Reduced-Matrigel (BD Falcon), 5 mg/cm^2 of fibronectin (BD Falcon), 5 mg/cm^2 of laminin (BD Falcon), 0.3 mg/ml of collagen (Nitta Gelatin) or 5% w/v BSA (Nacalai Tesque). After coating with ECM, 1×10^5 cells/ml were transferred to each pre-coated well and incubated for 24 h at 37°C. After washing two times with phosphate buffered saline (PBS), the floating and adherent cells were counted using trypan blue, and the number of adherent cells was divided by the number of floating cells to calculate the cell adherence ratios. In the neutralization experiments, the cells were pre-incubated with 20 mg/ml of anti-ITGA6, ITGB2, ITGB3 or ITGB4 antibodies prior to plating on the matrigel [33].

FACS analysis

The intensity of ITGB3, ITGB4 and ITGA6 expression in UCSD/AML1 and U937 cells was analyzed using FACSCalibur (BD Bioscience). The cells were stained with phycoerythrin (PE)-labeled anti-human ITGA6 (Clone: GoH3), ITGB4 (Clone: 58XB4) or ITGB3 (BI-PL2) antibodies purchased from Biolegend, Inc.

BrdU (Bromodeoxyuridine)/7-AAD (7-Aminoactinomycin D) staining

To assess the percentage of cells in sub G0/G1, G0/G1, and G2/M and S phase after 48 h of culture on matrigel or BSA-coated plates, 1×10^6 cells from each culture were fixed in BD Cytofix/Cytoperm buffer for 20 min., followed by a 300-mg/ml DNase treatment for 30 min. The cells were subsequently washed twice in BD Perm/Wash Buffer and stained with anti BrdU-APC (BD Biosciences/PharMingen, San Jose, CA) for 15 minutes, followed by staining with 7-AAD (BD Biosciences/PharMingen, San Jose, CA). The cells were harvested and analyzed using FACSCalibur with FL-4 (for BrdU-APC) and FL-3 (for 7-AAD) settings.

Ki67/7AAD staining

To assess the percentage of cells in G0 phase after 48 h of culture on matrigel or BSA-coated plates, 1×10^6 cells from each culture were fixed in 70% ethanol for 2 h, followed by a 2.5 μg/ml RNAse treatment for 30 minutes. The cells were subsequently washed twice in PBS/1% fetal bovine serum (FBS) and stained with mouse anti-human Ki67 (BD Biosciences/PharMingen, San Jose, CA) and Alexa647-conjugated anti-mouse IgG (Invitrogen) for 30 minutes, followed by staining with 7-AAD (BD Biosciences/PharMingen, San Jose, CA). The cells were harvested and analyzed using FACSCalibur with FL-4 (for Ki67-Alexa647) and FL-3 (for 7-AAD) settings.

Statistical analysis

Student's t-test was used to compare differences between the two groups.

Supporting Information

Figure S1 Expression of integrin genes and cell binding ability of various myeloid leukemia cells. A. The expression of 25 members of the integrin family was detected using semi-quantitative RT-PCR in HL60, U937, and K562 (cell lines with EVI1^{low} expression) and in UCSD/AML1, MOLM1, and HNT34 (cell lines with EVI1^{high} expression). The expression of EVI1 and b-actin in these cells is also shown. **B.** The expression of 18 genes in the integrin family was detected using RT-PCR in AML1/shLuc and AML1/shEVI1 cell lines. **C and D.** The adhesion ability of various HNT-34 cell lines (Pt, parental;/shLuc, transfection with small hairpin RNA for firefly luciferase;/shEVI1, transfection with small hairpin RNA for EVI1) to bind to matrigel is shown in C, and the expression of integrin genes in conjunction with EVI1 and b-actin is shown in D. **E and F.** The ability of PT9-related (PT9/shLuc and PT9/shEVI1) and PT11-related (PT11/shLuc and PT11/shEVI1) cell lines to bind to matrigel was measured (E), and the expression of various integrin genes in these four cell lines was determined using RT-PCR (F) **G.** The expression patterns of integrin genes were determined in U937/GFP and U937/EVI1 cell lines in conjunction with b-actin and EVI1.
(DOC)

Figure S2 Expression of various laminin chains in MC3T3-E1 cells. The relative expression levels of laminin a chains 1 to 5, laminin b chains 1 to 3, and laminin g chains 1 to 3 in MC3T3-E1 cells were determined using semi-quantitative RT-PCR.
(DOC)

Figure S3 Dose-response functions for AraC against four EVI1high AML cells. UCSD/AML1, MOLM1, PT9 and PT11 cells were incubated in BSA- or matrigel-coated wells of tissue culture plates and subsequently incubated with 10-3 to 10-7 M cytosine-arabinoside (Ara-C) for 48 h. Relative cell viability is calculated as a percentage relative to standard controls. Data are shown as mean ± S.E. Statistical analysis was performed using Student's t-test. A star (*) indicates $p<0.05$ and double stars (**) indicate $p<0.01$.
(DOC)

Figure S4 Drug sensitivity of EVI1^{high} and EVI1^{low} leukemia cells cultured with or without MC3T3-E1 cells determined by treatment with VP-16 or Ara-C. UCSD/AML1 (EVI1^{high}) leukemia cells and HL60 (EVI1^{low}) leukemia cells were treated with Ara-C or VP-16 for three days under plastic flasks (open diamonds) or co-cultured with MC3T3-E1 cells (closed squares); the viable cells were counted at each indicated time point. The percent cell viability compared to the number of untreated cells is shown for each indicated day. A star (*) indicates $p<0.05$.
(DOC)

Figure S5 Decreased cell growth with increased cell population in G0-phase of U937 cells with EVI1 expression cultured on the matrigel-coated plates. A. U937 cells were introduced by EVI1 expression vector (U937/EVI1) or control vector (U937/GFP) to determine their cell growths with culture condition on BSA or matrigel-coated plates. B and C. Cell cycle of U937/GFP as a control (B) and U937/EVI1 (C) were analyzed by BD FACSCalibur after double-stained by BrdU-APC and 7-AAD. Percentages of each cell cycles were shown by white bars (BSA-coated) and black bars (matrigel-coated). D. The percentage of cells in G0 phase in U937/EVI1 (black bars) and U937/GFP cells (white bars) cultured on matrigel- or BSA-coated plates were analyzed by BD FACSCalibur after double-stained by Ki67-Alexa647 and 7-AAD. Each experiment was performed in triplicate, and experiments were independently repeated at least

three times. Results are shown as mean ± S.E. Statistical analysis was performed using Student's t-test (**p<0.01; **p<0.05, vs control).
(DOC)

Figure S6 Expression profiles of ITGA6 and ITGB4 in AML patients. A and B. The expression patterns of ITGA6 (A) and ITGB4 (B) are shown as gene expression profiles for ten AML patients with EVI1low and ten AML patients with EVI1high expression (http://www.ncbi.nlm.nih.gov/geo, accession number GSE6891 [NCBI GEO]). C and D. The expression patterns of ITGA6 (C) and ITGB4 (D) are shown as gene expression profiles for patients in remission and for AML patients who had relapsed (http://www.ncbi.nlm.nih.gov/geo, accession number GDS1059 [NCBI GEO]).
(DOC)

Author Contributions

Conceived and designed the experiments: KM NY. Performed the experiments: NY KK YS. Analyzed the data: EI YS KM. Contributed reagents/materials/analysis tools: EI YS. Wrote the paper: KM NY KK.

References

1. Morishita K, Parker DS, Mucenski ML, Jenkins NA, Copeland NG, et al. (1988) Retroviral activation of a novel gene encoding a zinc finger protein in IL-3-dependent myeloid leukemia cell lines. Cell 54(6): 831–840.
2. Mucenski L, Taylor BA, Ihle JN, Hartley JW, Morse HC, 3rd, et al. (1988) Identification of a common ecotropic viral integration site, Evi-1, in the DNA of AKXD murine myeloid tumors. Mol Cell Biol 8(1): 301–308.
3. Morishita K, Parganas E, Bartholomew C, Sacchi N, Valentine MB, et al. (1990) The human Evi-1 gene is located on chromosome 3q24–q28 but is not rearranged in three cases of acute nonlymphocytic leukemias containing t(3;5)(q25;q34) translocations. Oncogene Res 5(3): 221–231.
4. Barjesteh van Waalwijk van Doorn-Khosrovani S, Erpelinck C, van Putten WL, Valk PJ, van der Poel-van de Luytgaarde S, et al. (2001) High EVI1 expression predicts poor survival in acute myeloid leukemia: a study of 319 de novo AML patients. Blood 101(3): 837–845.
5. Lugthart S, van Drunen E, van Norden Y, van Hoven A, Erpelinck CA, et al. (2008) High EVI1 levels predict adverse outcome in acute myeloid leukemia: prevalence of EVI1 over-expression and chromosome 3q26 abnormalities underestimated. Blood 111(8): 4329–4337.
6. Moroshita K (2007) Leukemogenesis of the EVI1/MEL1 gene family. Int J Hematol 85(4): 279–286.
7. Goyama S, Kurokawa M (2010) Evi-1 as a critical regulator of leukemic cells. Int J Hematol 91(5): 753–757.
8. Kurokawa M, Mitani K, Irie K, Matsuyama T, Takahashi T, et al. (1998) The oncoprotein Evi-1 represses TGF-β signalling by inhibiting Smad3. Nature 394(6688): 92–96.
9. Nitta E, Izutsu K, Yamaguchi Y, Imai Y, Ogawa S, et al. (2005) Oligomerization of Evi-1 regulated by the PR domain contributes to recruitment of corepressor CtBP. Oncogene 24: 6165–6173.
10. Palmer S, Brouillet JP, Kilbey A, Fulton R, Walker M, et al. (2001) Evi-1 transforming and repressor activities are mediated by CtBP co-repressor proteins. J Biol Chem 276(25): 834–840.
11. Yuasa H, Oike Y, Iwama A, Nishikata I, Sugiyama D, et al. (2005) Oncogenic transcription factor Evi1 regulates hematopoietic stem cell proliferation through GATA-2 expression. EMBO J 24(11): 1976–1987.
12. Shimahara A, Yamakawa N, Nishikata I, Morishita K (2010) Acetylation of lysine 564 adjacent to the C-terminal binding protein-binding motif in EVI1 is crucial for transcriptional activation of GATA2. J Biol Chem 285(22): 16967–16977.
13. Lvesque JP, Helwani FM, Winkler IG (2010) The endosteal 'osteoblastic' niche and its role in hematopoietic stem cell homing and mobilization. Leukemia 24(12): 1979–1992.
14. Wu JY, Scadden DT, Kronenberg HM (2009) Role of the osteoblast lineage in the bone marrow hematopoietic niches. J Bone Miner Res 24(5): 759–764.
15. Chan JY, Watt SM (2001) Adhesion receptors on heamatopoietic progenitor cells. Br J Haematol 112(3): 541–557.
16. Zhang J, Niu C, Ye L, Huang H, He X, et al. (2003) Identification of the haematopoietic stem cell niche and control of the niche size. Nature 425(6960): 836–841.
17. Zaidel-Bar R, Geiger B (2010) The switchable integrin adhesome. J Cell Sci 123(9): 1385–1388.
18. Desgrosellier JS, Cheresh DA (2010) Integrins in cancer: biological implications and therapeutic opportunities. Nat Rev Cancer 10(1): 9–22.
19. Papayannopoulou T, Craddock C, Nakamoto B, Priestley GV, Wolf NS (1995) The VLA4/VCAM-1 adhesion pathway defines contrasting mechanisms of lodgement of transplanted murine hemopoietic progenitors between bone marrow and spleen. PNAS 92(21): 9647–9651.
20. Papayannopoulou T, Nakamoto B (1993) Peripheralization of hemopoietic progenitors in primates treated with anti-VLA4 integrin. PNAS 90(20): 9374–9378.
21. Matsunaga T, Takemoto N, Sato T, Takimoto R, Tanaka I, et al. (2003) Interaction between leukemic-cell VLA-4 and stromal fibronectin is a decisive factor for minimal residual disease of acute myelogenous leukemia. Nat Med 9(9): 1158–1165.
22. Matsunaga T, Fukai F, Miura S, Nakane Y, Owaki T, et al. (2008) Combination therapy of an anticancer drug with the FNIII14 peptide of fibronectin effectively overcomes cell adhesion-mediated drug resistance of acute myelogenous leukemia. Leukemia 22(2): 353–60.
23. Becker PS, Kopecky KJ, Wilks AN, Chien S, Harlan JM, et al. (2009) Very late antigen-4 function of myeloblasts correlates with improved overall survival for patients with acute myeloid leukemia. Blood 113(4): 866–874.
24. Saito Y, Nakahata S, Yamakawa N, Kaneda K, Ichihara E, et al. (2011) CD52 as a molecular target for immunotherapy to treat acute myeloid leukemia with high EVI1 expression. Leukemia 25(4): 921–31.
25. Bergamini C, Sgarra C, Trerotoli P, Lupo L, Azzariti A, et al. (2007) Laminin-5 stimulates hepatocellular carcinoma growth through a different function of alpha6beta4 and alpha3beta1 integrins. Hepatology 46(6): 1801–1809.
26. Fortunel NO, Otu HH, Ng HH, Chen J, Mu X, et al. (2003) Comment on "'Stemness': transcriptional profiling of embryonic and adult stem cells" and "a stem cell molecular signature". Science 302(5644): 393.
27. Papayannopoulou T, Priestley GV, Nakamoto B, Zafiropoulos V, Scott LM (2001) Molecular pathways in bone marrow homing: dominant role of α4β1 over β2-integrins and selectins. Blood 98(8): 2403–2411.
28. Scott LM, Priestley GV, Papayannopoulou T (2003) Deletion of α4 integrins from adult hematopoietic cells reveals roles in homeostasis, regeneration, and homing. Mol Cell Biol 23(24): 9349–9360.
29. Verhaak RG, Wouters BJ, Erpelinck CA, Abbas S, Beverloo HB, et al. (2009) Prediction of molecular subtypes in acute myeloid leukemia based on gene expression profiling. Haematologica 94(1): 131–134.
30. Yagi T, Morimoto A, Eguchi M, Hibi S, Sako M, et al. (2003) Identification of a gene expression signature associated with pediatric AML prognosis. Blood 102(5): 1849–1856.
31. Lin KT, Yeh SH, Chen DS, Chen PJ, Jou YS (2005) Epigenetic activation of a4, b2 and b6 integrins involved in cell migration in trichostatin A-treated Hep3B cells. J Biomed Sci 12(5): 803–813.
32. Liu Y, Chen L, Ko TC, Fields AP, Thompson EA (2006) Evi1 is a survival factor which conveys resistance to both TGF-beta and taxol-mediated cell death via PI3K/AKT. Oncogene 25(25): 3565–3575.
33. Bei L, Lu Y, Bellis SL, Zhou W, Horvath E, et al. (2007) Identification of a HoxA10 Activation Domain Necessary for Transcription of the Gene Encoding beta 3 integrin during Myeloid Differentiation. J Biol Chem 282(23): 16846–16859.

Overexpression of the DNA sensor proteins, absent in melanoma 2 and interferon-inducible 16, contributes to tumorigenesis of oral squamous cell carcinoma with p53 inactivation

Yuudai Kondo,[1,2] Kentaro Nagai,[1,2] Shingo Nakahata,[2] Yusuke Saito,[2] Tomonaga Ichikawa,[2] Akira Suekane,[2] Tomohiko Taki,[3] Reika Iwakawa,[4] Masato Enari,[5] Masafumi Taniwaki,[3] Jun Yokota,[4] Sumio Sakoda[1] and Kazuhiro Morishita[2,6]

[1]Division of Oral and Maxillofacial Surgery, Medicine of Sensory and Motor Organs, and [2]Division of Tumor and Cellular Biochemistry, Department of Medical Sciences, Faculty of Medicine, University of Miyazaki, Miyazaki; [3]Department of Hematology and Oncology, Kyoto Prefectural University of Medicine, Kyoto; [4]Division of Multistep Carcinogenesis, and [5]Division of Refractory Cancer, National Cancer Center Research Institute, Tokyo, Japan

(Received September 1, 2011/Revised December 27, 2011/Accepted December 29, 2011/Accepted manuscript online February 9, 2012/Article first published online February 23, 2012)

The development of oral squamous cell carcinoma (OSCC) is a multistep process that requires the accumulation of genetic alterations. To identify genes responsible for OSCC development, we performed high-density single nucleotide polymorphism array analysis and genome-wide gene expression profiling on OSCC tumors. These analyses indicated that the absent in melanoma 2 (*AIM2*) gene and the interferon-inducible gene 16 (*IFI16*) mapped to the hematopoietic interferon-inducible nuclear proteins. The 200-amino-acid repeat gene cluster in the amplified region of chromosome 1q23 is overexpressed in OSCC. Both AIM2 and IFI16 are cytoplasmic double-stranded DNA sensors for innate immunity and act as tumor suppressors in several human cancers. Knockdown of AIM2 or IFI16 in OSCC cells results in the suppression of cell growth and apoptosis, accompanied by the downregulation of nuclear factor kappa-light-chain-enhancer of activated B cells activation. Because all OSCC cell lines have reduced p53 activity, wild-type p53 was introduced in p53-deficient OSCC cells. The expression of wild-type p53 suppressed cell growth and induced apoptosis via suppression of nuclear factor kappa-light-chain-enhancer of activated B cells activity. Finally, the co-expression of AIM2 and IFI16 significantly enhanced cell growth in p53-deficient cells; in contrast, the expression of AIM2 and/or IFI16 in cells bearing wild-type p53 suppressed cell growth. Moreover, AIM2 and IFI16 synergistically enhanced nuclear factor kappa-light-chain-enhancer of activated B cells signaling in p53-deficient cells. Thus, expression of AIM2 and IFI16 may have oncogenic activities in the OSCC cells that have inactivated the p53 system. (*Cancer Sci* 2012; 103: 782–790)

Oral squamous cell carcinoma is commonly found in low-income communities. This cancer mainly affects older men; 90% of cases are in men over 45 years old who have been exposed to risk factors including tobacco and/or alcohol (International Agency for Research on Cancer [IARC] 2004). OSCC is the sixth most common cancer worldwide and affects approximately 270 000 people each year.[1] The incidence and rate of mortality from OSCC are rising in several regions of Europe, Australia and Asia, including Japan. Despite recent progress in OSCC diagnosis and therapy, the 5-year survival rate has not improved in more than two decades.[2]

Oral carcinogenesis is a multifactorial cascade involving numerous genetic changes that affect the activity of oncogenes, tumor suppressor genes and other classes of disease-related genes. Chronic exposure to carcinogens, such as tobacco, causes genetic changes in the epithelial cells of the oral mucosa. The activation of the *COX-2*,[3] epidermal growth factor receptor,[4] and cyclin D1 oncogenes and the inactivation of the *p16* and *p53* tumor suppressor genes have also been reported in OSCC.[5–7] In addition to tobacco smoke exposure, chronic alcohol use and chronic inflammation can both induce genetic alterations.[3] The causative agent of cervical cancer, HPV is also reportedly associated with head and neck cancers, including OSCC.[8] Compared to HPV-negative cases, HPV-positive OSCC have an intact *p16* gene and wild-type *p53*, and harbor frequent genetic alterations of the *p16* and *p53* genes.[9,10] The HPV oncoproteins E6 and E7 exploit the ubiquitin-proteasome system to degrade and functionally inactivate negative cell-regulatory proteins, including members of the p110 (Rb) family and p53; this process may primarily contribute to HPV-induced carcinogenesis.[11]

The innate immune system provides nonspecific protection and enhances the adaptive immune response against a variety of pathogens, including HPV. The IFI16 and AIM2 proteins were recently found to be innate immune sensors for cytosolic dsDNA. Upon sensing dsDNA, the IFI16 protein induces the expression of IFN-β,[12] whereas the AIM2 protein forms an inflammasome that promotes the secretion of interleukin-1β.[13] Both *IFI16* and *AIM2* belong to the HIN-200 gene family found on human and mouse chromosome 1; they are positively regulated by type I and II INF and have been described as regulators of cell proliferation, differentiation, apoptotic and inflammatory processes.[14] The overexpression of IFI16 in cells inhibits cell proliferation by potentiating the p53/p21- and Rb/E2F-mediated inhibition of cell-cycle progression, and IFI16 downregulation contributes to oncogenesis.[15,16] Also, AIM2 expression suppresses cell proliferation and tumorigenicity of human breast cancer cells.[17] Therefore, it has been proposed that *AIM2* and *IFI16* function as tumor suppressor genes.

To identify genes involved in OSCC tumorigenesis, OSCC tumors were submitted to genomic analysis by high-density SNP array analysis. A number of amplified or deleted genomic regions in OSCC cells were identified, and a series of genes in the genetically altered regions were selected by expression

[6]To whom correspondence should be addressed.
E-mail: kmorishi@med.miyazaki-u.ac.jp

doi: 10.1111/j.1349-7006.2012.02211.x

profile analysis. Of these genes, the NIH-200 gene family locus on chromosome 1q23 was frequently amplified, and *AIM2* and *IFI16* in the NIH-200 gene family were highly expressed in most OSCC tumors. Although *AIM2* and *IFI16* were reported to be tumor suppressors, the expression of AIM2 and IFI16 enhanced the cell growth of OSCC cell lines. Here we describe a mechanism by which *AIM2* and *IFI16* may be functioning as oncogenes in OSCC.

Materials and Methods

Materials and Methods are given in Data S1 and Data S2 in the supporting information.

Results

Higher expression of AIM2 and IFI16 with frequent amplification at 1q23 in OSCC. To identify novel genes responsible for tumorigenesis in OSCC, we performed high-density SNP array analysis on 28 OSCC tumor samples using an Affymetrix Human Mapping 250K Sty Array (Affymetrix, Santa Clara, CA, USA). The most frequent gains involved segments of chromosomes 1, 3q, 5p, 6p, 7p, 8q, 9q, 14, 15, 16, 17, 19, 20 and 22, whereas the most frequent losses involved segments of chromosomes 3p, 4, 5q, 8p, 10p, 18q and 21q (Fig. S1). Of these, 77 were amplified and ranged in size from 0.3 to 49.3 Mb, and four were found to be deleted and ranged in size from 0.2 to 0.6 Mb, in more than 14 of 28 OSCC tumor samples (Table S1).

To select candidate genes within the regions with altered copy numbers, we analyzed a data set from the NCBI Gene Expression Omnibus (http://www.ncbi.nlm.nih.gov/geo/), which contained the gene expression data of four oral tissue samples from healthy volunteers and 16 tumor samples from OSCC patients.[18] Of the genes in the amplified regions, 27 were expressed at more than two-fold higher levels ($P < 0.01$) (Table S1-1). However, no genes that were downregulated more than two-fold were identified in the deleted region (Table S1 2). Interestingly, 15 of the 27 candidates were previously reported to be cancer-related genes. The genes linked to OSCC included keratin 19, lectin, galactoside-binding, soluble, 1 and *IFI16*.[19–21] Furthermore, five of the 27 upregulated genes were also found to be *IFI* genes, including *IFI6*, *IFI35*, *AIM2*, *IFI16* and bone marrow stromal cell antigen-2. Among them, the *AIM2* and *IFI16* genes are located within the HIN-200 gene cluster on 1q23 and have been identified as a new family of innate immune DNA sensors for intracellular DNA called AIM2-like receptors.[12] Because chronic inflammation and infection contribute to the development of several types of cancer, we analyzed the HIN-200 gene cluster locus on 1q23.

Based on the SNP array analysis from 28 OSCC cases, four members of the HIN-200 family, along with other 19 genes, were located in the 1.3-Mb common region of amplification at 1q23 (Fig. 1a). The expression profiles showed that IFI16 and AIM2 are highly expressed in OSCC, but no significant differences in the expression levels of the other 21 genes, including myeloid cell nuclear differentiation antigen (*MNDA*) and pyrin and HIN domain family, member 1 (*PYHIN*), were observed between the OSCC and control oral tissues (Fig. S2a–c). Using semi-quantitative and quantitative real-time PCR, we confirmed statistically significant higher expression of AIM2 and IFI16 in tumor samples from OSCC patients and OSCC cell lines ($P < 0.05$) (Figs 1b–e, S2d). Moreover, the expression of AIM2 was significantly higher in the group with metastasis (N1) than in that without metastasis (N0) ($P < 0.05$). To confirm the relationship between genomic amplification and mRNA expression levels of *AIM2* and *IFI16*, a scatter plot was used to evaluate the correlation between the two variables in 20 OSCC tumor samples and eight cell lines. As shown in Figure 1(f), we found weak but positive correlations between the DNA copy numbers and mRNA expression levels for the two genes. Although a few cases did not show gene amplification or overexpression of the *AIM2* and *IFI16* genes, the majority of cases presented gene amplification and high expression of these two genes. Thus, in the HIN-200 family of genes, *AIM2* and *IFI16*, are overexpressed in OSCC, and this overexpression is frequently accompanied by gene amplification.

High expression of AIM2 and IFI16 enhanced cell growth by preventing apoptosis in OSCC cells. An important inflammasome component, AIM2 senses potentially dangerous cytoplasmic DNA and regulates caspase-1 activation.[13] Cytoplasmic overexpression of AIM2 also reportedly reduces cell proliferation and increases susceptibility to cell death in transfected murine fibroblasts. To determine whether the high expression levels of AIM2 or IFI16 have an effect on OSCC cell growth, we introduced an shRNA expression vector against AIM2 (shAIM2), IFI16 (shIFI16) or luciferase (shLuc) as a control into the human OSCC cell line SAS. SAS cells expressing the shRNA for either AIM2 (SAS/shAIM2) or IFI16 (SAS/shIFI16) had decreased growth rates relative to control-transfected cells (SAS/shLuc) (Fig. 2a,b). Notably, downregulation of both AIM2 and IFI16 expression had the most significant effect on growth inhibition. Similar effects were observed in the HSC4-OSCC cell line (Fig. S3). Next, apoptosis and cell cycle were investigated by flow cytometry with propidium iodide (PI) and Annexin V, respectively. The cell cycle profiles of SAS/shAIM2 and SAS/shIFI16 cells were not significantly different from those of the control SAS/shLuc cells, but the SAS/shAIM2 and SAS/shIFI16 cells exhibited a higher percentage of cell death (sub-G1 population) than the SAS/shLuc cells (Figs 2c, S4). In the SAS/shAIM2 and SAS/shIFI16 cells, the percentage of cells that bound Annexin V increased approximately 10- and 3-fold, respectively, compared with the SAS/shLuc cells (Fig. 2d). These data suggest that high expression of AIM2 and IFI16 enhances cell survival by preventing OSCC cells from entering apoptosis.

Activation of NF-κB signaling by AIM2 and IFI16 in OSCC. Once bound to the DNA in the cytoplasm, AIM2 activates both NF-κB and caspase-1,[13] and cytosolic DNA also triggers NF-κB activation by IFI16.[12] To clarify the mechanisms by which constitutive expression of AIM2 and/or IFI16 prevent apoptosis in OSCC cells, we studied caspase-1 and NF-κB for constitutive activation in OSCC. Initially, the SAS-OSCC cell lines transfected with the shLuc, shIFI16 or shAIM2 vectors were examined for the expression of cleaved caspase-1 by immunoblot analysis using a cleaved caspase-1 specific antibody. Cleaved caspase-1 was not detected in any of these cell lines but was detected in the human acute monocytic leukemia cell line (THP-1) transfected with poly deoxyadenylic-deoxythymidylic acid (poly[dA:dT]) as a positive control (Fig. S5a). The cleaved form of caspase-1 was also not detected in seven of the eight OSCC cell lines except for HSQ89 (data not shown). In addition, the treatment of SAS-OSCC cells with poly(dA:dT) had no effect on caspase-1 cleavage (Fig. S5b), suggesting that dsDNA could not trigger the formation of the AIM2 inflammasome in OSCC cells.

To assess NF-κB activation in OSCC, we measured IκBα protein in eight OSCC cell lines and 10 primary OSCC tumors by immunoblot analysis. We observed significantly higher levels of phosphorylated IκBα and lower levels of total IκBα in most OSCC cell lines and primary tumor samples compared to control gingival tissues (Fig. 3a). This result suggests that NF-κB signaling is often activated in OSCC. To confirm this hypothesis, four OSCC cell lines (HSQ89, HSC3, HSC4 and SAS) were treated with various concentrations of the NF-κB

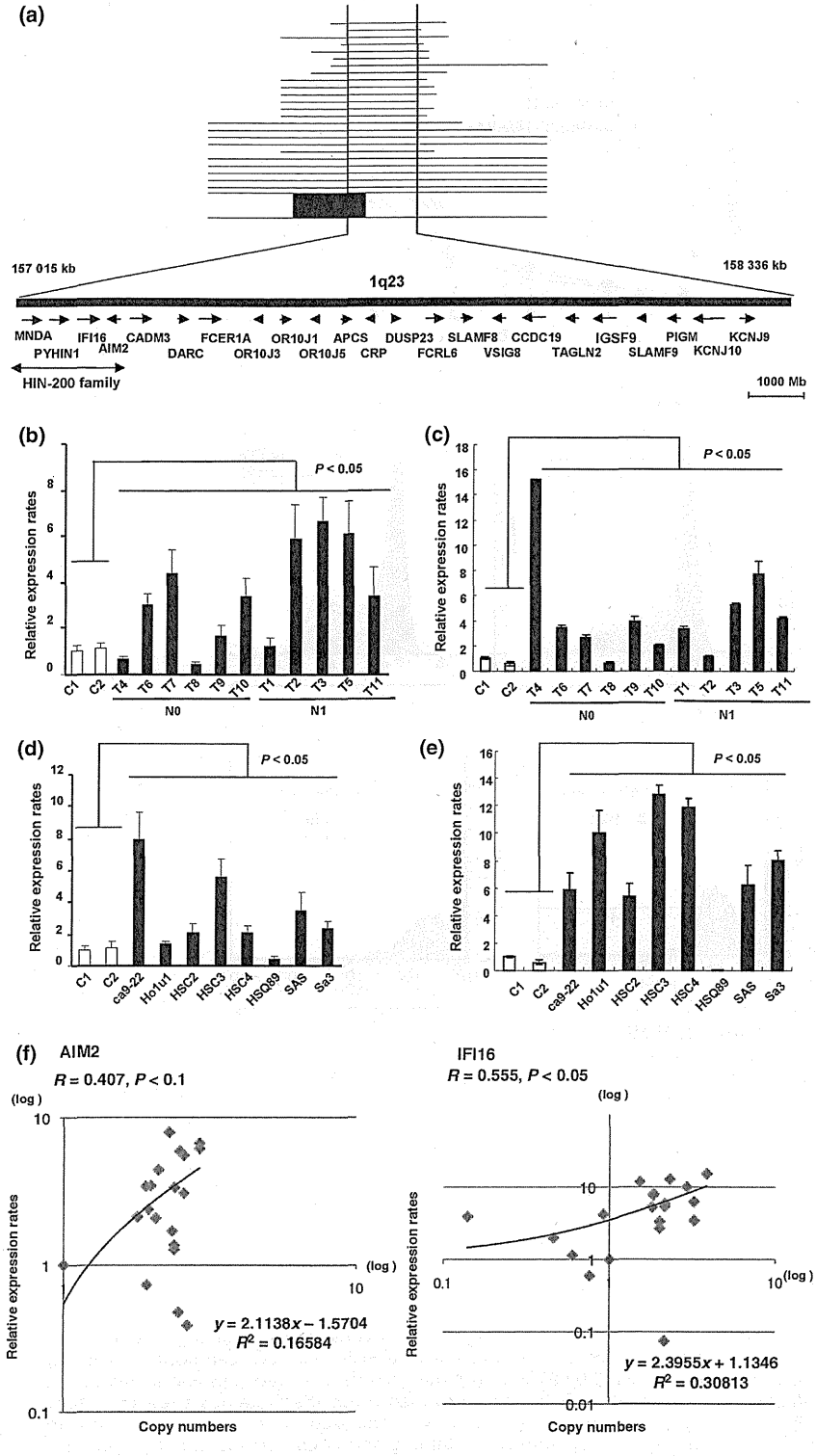

Fig. 1. Overexpression of IFI16 and AIM2 mRNA in OSCC. (a) Recurrent genetic changes are depicted based on the copy number analyzer for GeneChip (CNAG) output of the single nucleotide polymorphism array analysis of 28 oral squamous cell carcinoma (OSCC) samples, which include gains at the *IFI16* and *AIM2* loci on 1q23. Regions showing copy number gains are indicated by horizontal lines. *AIM2*, absent in melanoma 2; *APCS*, amyloid P component, serum; *CADM3*, cell adhesion molecule 3; *CCDC19*, coiled-coil domain containing 19; *CRP*, C-reactive protein, pentraxin-related; *DARC*, Duffy blood group, chemokine receptor; *DUSP23*, dual specificity phosphatase 23; *FCER1A*, Fc fragment of IgE, high affinity I, receptor for: alpha polypeptide; *FCRL6*, Fc receptor-like 6; *IFI16*, interferon, gamma-inducible protein 16; *IGSF9*, immunoglobulin superfamily, member 9; *KCNJ9*, potassium inwardly-rectifying channel, subfamily J, member 9; *KCNJ10*, potassium inwardly-rectifying channel, subfamily J, member 10; *MNDA*, myeloid cell nuclear differentiation antigen; *OR10J1*, olfactory receptor, family 10, subfamily J, member 1; *OR10J3*, olfactory receptor, family 10, subfamily J, member 3; *OR10J5*, olfactory receptor, family 10, subfamily J, member 5; *PIGM*, phosphatidylinositol glycan anchor biosynthesis, class M; *PYHIN1*, pyrin and HIN domain family, member 1; *SLAMF8*, SLAM family member 8; *SLAMF9*, SLAM family member 9; *TAGLN2*, transgelin 2; *VSIG8*, V-set and immunoglobulin domain containing 8. (b,d) Expression of the AIM2 and (c,e) IFI16 mRNA were examined in 11 primary OSCC and eight OSCC cell lines (Ca9-22, Ho1u1, HSC2, HSC3, HSC4, HSQ89, SAS and Sa3) by quantitative real-time PCR. Normal gingival tissues from normal volunteers were used as controls. (f) Scatter plot of DNA copy number versus mRNA expression for *AIM2* (left) and *IFI16* (right). Correlations were quantified using the Spearman's rank correlation coefficient. AIM2, absent in melanoma; HIN-200, Hematopoietic interferon-inducible nuclear proteins with a 200-amino-acid repeat; IFI16, interferon-inducible 16; N0, without metastasis; N1, with metastasis.

inhibitor Bay 11-7082 for 48 h and examined for cell viability. In three of the four cell lines (not HSQ89), cell viability was inhibited by Bay 11-7082 treatment, although the effect varied among the cell lines (Fig. 3b). To determine whether the observed cell death was due to apoptosis, two cell lines, SAS and HSC3, treated with or without Bay 11-7082 were stained with Annexin V/PI and analyzed by flow cytometry. Over 90% of the OSCC cell lines underwent apoptosis 48 h after treatment with 10-μM Bay11-7082 (Figs 3c, S6). Moreover, there was a dose-dependent increase in the total IκBα and decrease in the phosphorylated IκBα levels after exposure to 1–10-μM Bay11-7082 (Fig. 3d). To determine whether high expression of AIM2 and/or IFI16 contributes to the constitutive NF-κB activation in OSCC, SAS cells were transfected with either shIFI16 and/or shAIM2 vectors and analyzed for IκBα expression. As expected, the SAS cells treated with shIFI16, shAIM2 or both shRNA significantly increased protein levels of phosphorylated-IκBα and reduced the total IκBα levels compared with control cells transfected with shLuc and parental cells (Fig. 3e). The reduction of NF-κB activation by shIFI16 or

doi: 10.1111/j.1349-7006.2012.02211.x

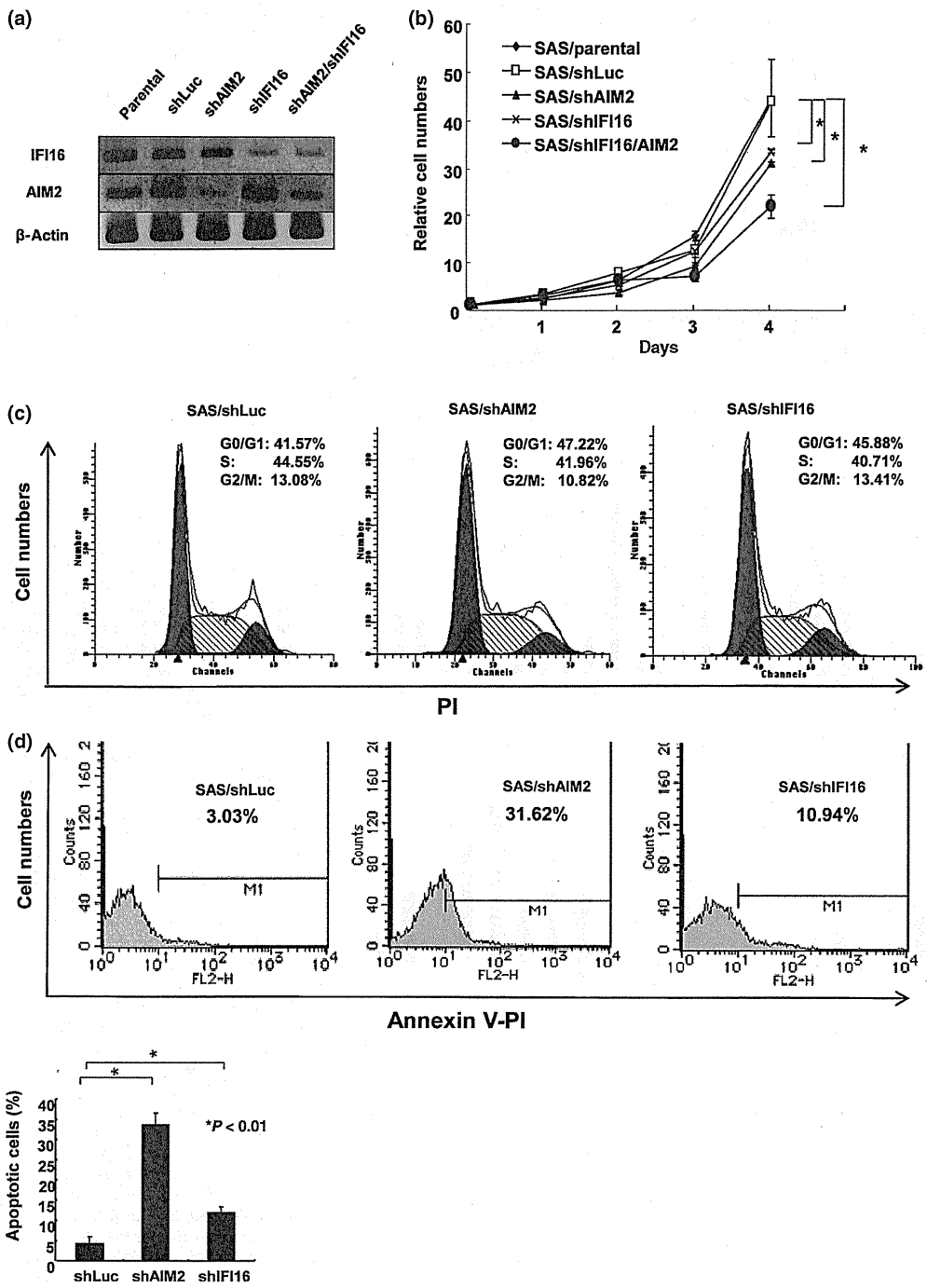

Fig. 2. Effects of knockdown of AIM2 and IFI16 expression on the growth of OSCC cells. (a) Retroviral constructs containing shRNA against AIM2 and/or IFI16 or luciferase (Luc) as a control were transfected into SAS cells. Forty-eight hours after transfection, ZsGreen-positive cells were sorted, and total RNA was extracted to analyze expression levels of AIM2 and IFI16 by RT-PCR. (b) The growth of sorted cells was analyzed with MTT. The data are shown as the mean ± SD of triplicate samples. The statistical analysis was performed using the Student's *t*-test (*$P < 0.01$). (c) Cell cycle phase distribution was analyzed by FACS with PIstaining. Each cycle phase distribution was analyzed by the cell recruited into the cell cycle. (d) The percentage of sorted cells undergoing apoptosis was quantitated by Annexin V staining and FACS. The lower bar graph shows the mean ± SD from three independent experiments. An asterisk indicates a statistically significant difference ($P < 0.01$). AIM2, absent in melanoma; IFI16, interferon-inducible 16.

shAIM2 was also confirmed by NF-κB-dependent luciferase reporter activity assay (Fig. 3f). The overexpression of IFI16 and AIM2 may enhance IκBα kinase activity and promote the degradation of IκBα and NF-κB activation, leading to the acceleration of cell growth in OSCC cells.

Restoration of p53 function inhibits constitutive NF-κB activation in OSCC cells. Studies have reported that the overexpression of HIN-200 proteins can decrease cell proliferation and block cell cycle progression at the G1-S phase transition.[14] It has been shown that IFI16-mediated growth arrest is partly dependent on

the function of p53.[15] Because a high frequency of mutations in p53 was noted in OSCC,[22] we determined whether p53 dysfunction results in abrogation of the growth suppressive effects of AIM2 and IFI16 in OSCC cells. Initially, we determined the expression and genomic alterations of p53 in eight OSCC cell lines. All cell lines showed p53 point mutations (Table S2-1, Doc. S2) and five (Ca9-22, HSC4, HSQ89, SAS and Sa3) expressed a detectable level of p53 protein, including a truncated form of p53 (Fig. 4a).[20,21] In primary OSCC samples, five out of 11 tumors had abnormally high expression levels and/or point mutations of p53 (data not shown) (Table S2-2). We introduced the wild-type p53 expression vector into the SAS cell line and confirmed that the expression of wild-type p53 decreased the growth rate of SAS cells (Fig. 4b,c). The percentage of Annexin V-positive cells significantly increased in wild-type p53-transfected cells (Fig. 4d), indicating that this p53-mediated growth suppression of SAS cells is associated with apoptosis.

It has been reported that p53 regulates glucose metabolism through the NF-κB pathway, and both basally expressed and genotoxicity-activated p53 inhibits the activity of IκB kinase and the transcriptional activity of NF-κB.[23] Therefore, we determined whether p53 could inhibit NF-κB activation in OSCC cells. A significant increase in the IκBα protein level and a decrease in phosphorylated IκBα were observed when SAS cells were transfected with wild-type p53 (Fig. 4e). Wild-type p53 also inhibited the basal NF-κB reporter activity of SAS cells (Fig. 4f). These data suggest that constitutive activation of the NF-κB pathway in OSCC is partly due to a loss of p53 function.

The overexpression AIM2 and IFI16 synergistically promotes cell growth only in the absence of functional p53. To determine whether a lack of functional p53 is associated with the growth-promoting effect of AIM2 and IFI16 in OSCC cells, we transfected human lung cancer H1299 cells, which lack endogenous p53,[24] with various combinations of the AIM2, IFI16 and p53 expression vectors. The transfection of AIM2, IFI16, or p53 alone had no significant effect on the growth rate of H1299 cells (Fig. 5a,b). However, co-transfection of AIM2 and IFI16 strongly promoted cell proliferation with increased IκBα phosphorylation. Strikingly, the growth-promoting effect of AIM2 and IFI16 was abrogated in the presence of wild-type p53. To further confirm these results, we performed cell proliferation assays using the human mammary tumor cell line MCF-7 expressing wild-type p53, which has been used to study the role of IFI16 in p53-dependent apoptosis.[25] Transfection with either or both of the AIM2 and IFI16 expression vectors retarded the growth rate of MCF-7 cells. The shRNA inhibition of p53 expression caused a slight increase in cell growth rate (Fig. 5c,d). Importantly, co-transfection of AIM2 and IFI16 with a shRNA expression vector for p53 led to an approximately two-fold higher proliferation rate with significant upregulation of phosphorylated IκBα. Thus, the simultaneous high expression of AIM2 and IFI16 confers a proliferative advantage in cells with functionally inactive p53, in part, through the activation of NF-κB signaling.

Finally, we examined whether co-expression of both AIM2 and IFI16 can activate NF-κB in an OSCC cell line. Very low expression levels of AIM2 and IFI16 and a low level of NF-κB

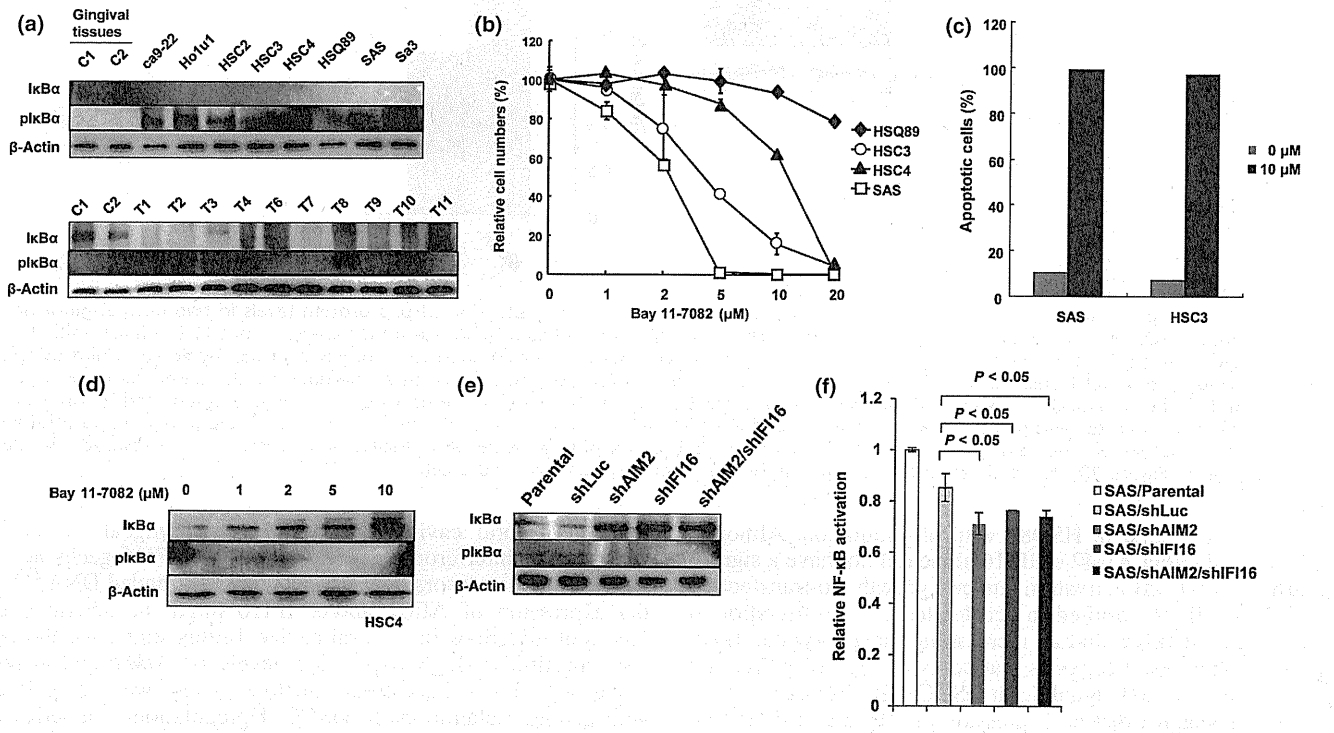

Fig. 3. Activation of NF-κB signaling in oral squamous cell carcinoma (OSCC). (a) The levels of total and phosphorylated (Ser32/36) inhibitor of kappa B alpha (IκBα) were examined in two normal gingival tissue samples, eight OSCC cell lines (Ca9-22, Ho1u1, HSC2, HSC3, HSC4, HSQ89, SAS and Sa3) and 10 OSCC primary tumors by Western blot analysis. (b) Four OSCC cell lines were treated with various concentrations of Bay 11-7082 for 48 h, and viable cell numbers were counted by MTT assay. The results are shown as percentages of the values obtained from the control Bay 11-7082-free culture. The data are shown as the means ± SD of triplicate samples. (c) The percentage of apoptotic cells was measured by FACS after Annexin V/PI staining in untreated and 10-μM Bay 11-7082-treated SAS and HSC3 cell lines at 48 h. (d) Levels of phosphorylated IκBα and total IκBα in the HSC4 cell line treated with the indicated concentration of Bay 11-7082 for 48 h were examined by Western blot analysis. (e) The SAS cell transfectants described in Figure 2 were examined for the levels of phosphorylated IκBα and total IκBα by Western blot analysis. (f) The SAS cell transfectants were co-transfected with the NF-κB–Luc reporter and an internal control Renilla luciferase (pRL-TK) plasmid. After 36 h, luciferase activities were measured with a dual-luciferase reporter assay system. The data are shown as mean ± SD of triplicate transfections, and statistical analysis used the Student's *t*-test. NF-κB, nuclear factor kappa-light-chain-enhancer of activated B cells.

doi: 10.1111/j.1349-7006.2012.02211.x

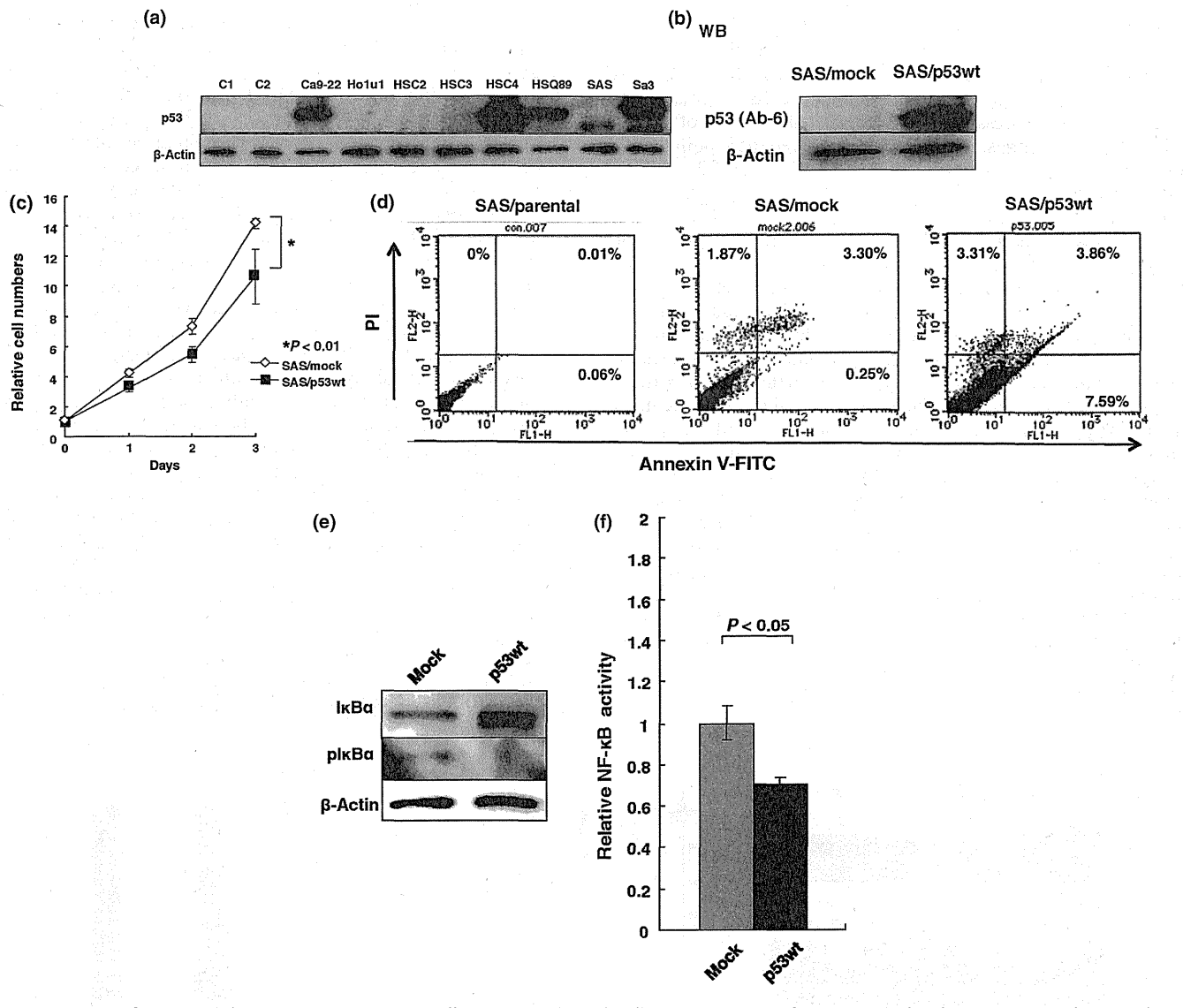

Fig. 4. Function of p53 is inhibited in oral squamous cell carcinoma (OSCC) cells. (a) Detection of p53 protein levels in two normal gingival tissues and in eight OSCC cell lines (Ca9-22, Ho1u1, HSC2, HSC3, HSC4, HSQ89, SAS and Sa3) by Western blot analysis. (b) SAS cell lines stably transfected with either empty vector or wild-type p53 expression vector (FLAG-p53wt) were examined for expression of p53 by Western blot using an anti-p53 antibody (Ab-6). (c) Transfectants were subjected to cell growth analysis using the MTT assay. The data are shown as the mean ± SD of triplicate samples. The statistical analysis was done using the Student's *t*-test. (d) The percentage of apoptotic cells was quantified by Annexin-V/PI staining. (e) Control vector and p53 transfectants were examined for levels of phosphorylated inhibitor of kappa B alpha (IκBα) and total IκBα by Western blot analysis. (f) The cells were co-transfected with NF-κB–Luc and pRL-TK. After 36 h, luciferase activities were measured. The data are presented as in Figure 3(f). NF-κB, nuclear factor kappa-light-chain-enhancer of activated B cells.

activation were found in HSQ89 with p53 mutation. Although transfection of either AIM2 or IFI16 alone did not have a significant effect on NF-κB activation and cell growth, co-transfection of AIM2 and IFI16 resulted in accelerated cell proliferation, a decrease in total IκBα, and an increase in phosphorylated IκBα (Fig. 5e,f). This result suggests that co-expression of AIM2 and IFI16 activates NF-κB signaling in OSCC cells. Taken together, these results suggest that co-expression of AIM2 and IFI16 can promote cell proliferation through activation of NF-κB signaling pathway in the absence of p53.

Discussion

The oral cavity contains some of the most varied and extensive flora in the entire human body. A member of a group of DNA-based viruses, HPV infects the skin and mucous membranes within the human body. Infection with HPV 16 and 18 increases the risk of oral cavity cancer and oropharyngeal cancer.[11] Because the interferon-inducible *AIM2* and *IFI16* genes act as innate immune sensors for cytosolic double-stranded DNA,[12,13] the expression of AIM2 and/or IFI16 might be activated by recurrent infections in the oral cavity. In this study, we showed that constitutive high expression levels of *AIM2* and *IFI16*, along with other interferon-inducible genes, were associated with genomic alterations in OSCC. Upregulation of a series of interferon-inducible genes and enhancement of interferon-signaling pathways has previously been reported in OSCC by protein expression analysis using tandem mass spectrometry or by mRNA expression profile analysis using a DNA microarray.[26,27] The expression of the interferon-inducible gene is an important characteristic of OSCC. Moreover, OSCC cells were shown to become resistant to IFN-β-mediated inhibition of cell growth.[26] The constitutive expression of the interferon-inducible genes may affect the development of OSCC, and the expres-

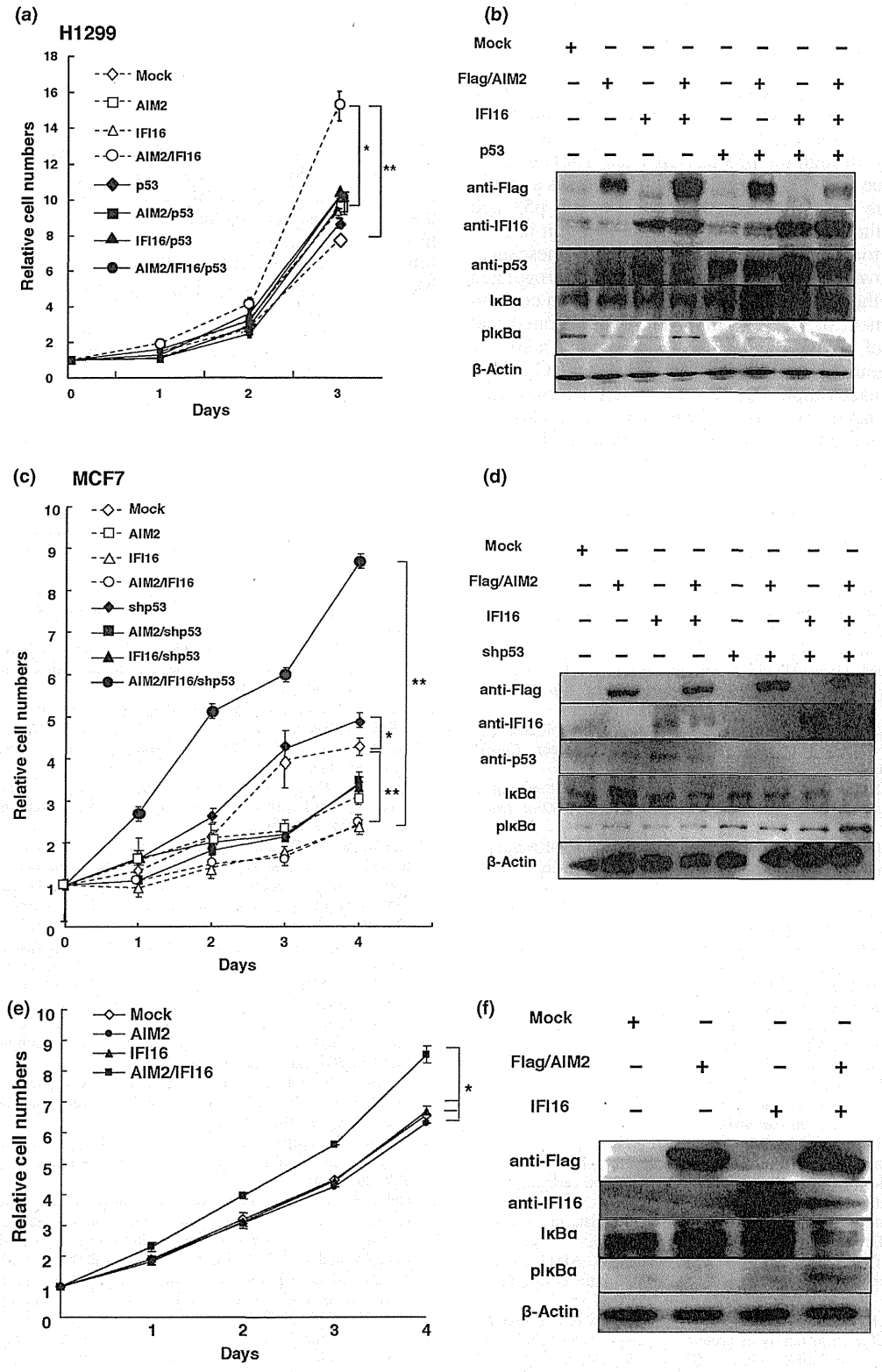

Fig. 5. Expression of AIM2 and IFI16 confers growth-stimulating effects on transformed cells in the absence of wild-type p53. (a) The growth of human lung cancer H1299 cells after transfection with various combinations of AIM2, IFI16 and wild-type p53 (SN3-p53wt) expression vectors was examined by MTT assay. The data are shown as the mean ± SD of triplicate samples. The statistical analysis was performed using the Student's *t*-test (*$P < 0.05$; **$P < 0.01$). (b) Western blot analysis of extracts from untransfected or transfected H1299 cells described in panel (a) at 48 h. (c) The growth of human mammary tumor MCF7 cells after transfection with various combinations of the AIM2, IFI16 and shp53 expression vectors was examined by MTT assay. The data are shown as the mean ± SD of triplicate samples. The statistical analysis was performed using the Student's *t*-test (*$P < 0.05$; **$P < 0.01$). (d) Western blot analysis of extracts from untransfected or transfected MCF7 cells described in panel (c) at 48 h. (e) The growth of HSQ89 cells after transfection with AIM2 and/or IFI16. (f) Western blot analysis of extracts from untransfected or transfected HSQ89 cells described in panel (e) at 48 h. AIM2, absent in melanoma; IκBα, inhibitor of kappa B alpha; IFI16, interferon-inducible 16.

doi: 10.1111/j.1349-7006.2012.02211.x

sion of a subset of the interferon-inducible genes may arise as a result of genomic alterations.

Although the *AIM2* and *IFI16* genes were thought to be tumor suppressors in a series of cancers, high expression levels of AIM2 and IFI16 enhanced the cell growth and prevented apoptosis in OSCC. In normal aged human cells, increased levels of the IFI16 protein reportedly contribute to senescence-associated cell growth arrest partly through the p53/p21CIP1 and Rb/E2F pathway and upregulation of IFI16 expression by p53. This is a part of a component of the positive feedback loop between p53 and IFI16.[28] Because the loss of p53 and/or IFI16 function in cells has been suggested to contribute to defects in cellular senescence-associated cell growth arrest, we speculate that dysregulated IFI16 function together with the loss of p53 function can contribute to the development of OSCC. This study demonstrated that the co-expression of AIM2 and IFI16 synergistically activates NF-κB signaling, and the activation of NF-κB in OSCC is also dependent on p53 inactivation. Future studies will determine the precise activation mechanisms of NF-κB signaling and/or the transcriptional activity of IFI16 in OSCC with inactivated p53.

Disclosure Statement

The authors have no conflict of interest to declare.

Abbreviations

AIM2	absent in melanoma 2
HIN-200	hematopoietic interferon-inducible nuclear proteins with a 200-amino-acid repeat
HPV	human papillomavirus
IFI	interferon-inducible
IFN	interferon
IκBα	inhibitor of kappa B alpha
NF-κB	nuclear factor kappa-light-chain-enhancer of activated B cells
OSCC	oral squamous cell carcinoma
SNP	single-nucleotide polymorphism

References

1 Shah JP, Singh B. Keynote comment: why the lack of progress for oral cancer? *Lancet Oncol* 2006; **7**: 356–7.
2 Gibson MK, Forastiere AA. Reassessment of the role of induction chemotherapy for head and neck cancer. *Lancet Oncol* 2006; **7**: 565–74.
3 Perez-Sayans M, Somoza-Martin JM, Barros-Angueira F, Reboiras-Lopez MD, Gandara Rey JM, Garcia-Garcia A. Genetic and molecular alterations associated with oral squamous cell cancer (Review). *Oncol Rep* 2009; **22**: 1277–82.
4 Rogers SJ, Harrington KJ, Rhys-Evans P, P OC, Eccles SA. Biological significance of c-erbB family oncogenes in head and neck cancer. *Cancer Metastasis Rev* 2005; **24**: 47–69.
5 Rousseau A, Lim MS, Lin Z, Jordan RC. Frequent cyclin D1 gene amplification and protein overexpression in oral epithelial dysplasias. *Oral Oncol* 2001; **37**: 268–75.
6 Reed AL, Califano J, Cairns P *et al.* High frequency of p16 (CDKN2/MTS-1/INK4A) inactivation in head and neck squamous cell carcinoma. *Cancer Res* 1996; **56**: 3630–3.
7 Choi S, Myers JN. Molecular pathogenesis of oral squamous cell carcinoma: implications for therapy. *J Dent Res* 2008; **87**: 14–32.
8 Sisk EA, Soltys SG, Zhu S, Fisher SG, Carey TE, Bradford CR. Human papillomavirus and p53 mutational status as prognostic factors in head and neck carcinoma. *Head Neck* 2002; **24**: 841–9.
9 Min BM, Baek JH, Shin KH, Gujuluva CN, Cherrick HM, Park NH. Inactivation of the p53 gene by either mutation or HPV infection is extremely frequent in human oral squamous cell carcinoma cell lines. *Eur J Cancer B Oral Oncol* 1994; **30B**: 338–45.
10 Boyer SN, Wazer DE, Band V. E7 protein of human papilloma virus-16 induces degradation of retinoblastoma protein through the ubiquitin-proteasome pathway. *Cancer Res* 1996; **56**: 4620–4.
11 Feller L, Wood NH, Khammissa RA, Lemmer J. Human papillomavirus-mediated carcinogenesis and HPV-associated oral and oropharyngeal squamous cell carcinoma. Part 1: human papillomavirus-mediated carcinogenesis. *Head Face Med* 2010; **6**: 14.
12 Unterholzner L, Keating SE, Baran M *et al.* IFI16 is an innate immune sensor for intracellular DNA. *Nat Immunol* 2010; **11**: 997–1004.
13 Fernandes-Alnemri T, Yu JW, Datta P, Wu J, Alnemri ES. AIM2 activates the inflammasome and cell death in response to cytoplasmic DNA. *Nature* 2009; **458**: 509–13.
14 Asefa B, Klarmann KD, Copeland NG, Gilbert DJ, Jenkins NA, Keller JR. The interferon-inducible p200 family of proteins: a perspective on their roles in cell cycle regulation and differentiation. *Blood Cells Mol Dis* 2004; **32**: 155–67.
15 Ludlow LE, Johnstone RW, Clarke CJ. The HIN-200 family: more than interferon-inducible genes? *Exp Cell Res* 2005; **308**: 1–17.
16 Liao JC, Lam R, Brazda V *et al.* Interferon-inducible protein 16: insight into the interaction with tumor suppressor p53. *Structure* 2011; **19**: 418–29.
17 Chen IF, Ou-Yang F, Hung JY *et al.* AIM2 suppresses human breast cancer cell proliferation in vitro and mammary tumor growth in a mouse model. *Mol Cancer Ther* 2006; **5**: 1–7.
18 Toruner GA, Ulger C, Alkan M *et al.* Association between gene expression profile and tumor invasion in oral squamous cell carcinoma. *Cancer Genet Cytogenet* 2004; **154**: 27–35.
19 Zhong LP, Zhao SF, Chen GF, Ping FY, Xu ZF, Hu JA. Increased levels of CK19 mRNA in oral squamous cell carcinoma tissue detected by relative quantification with real-time polymerase chain reaction. *Arch Oral Biol* 2006; **51**: 1112–9.
20 Ding YM, Dong JH, Chen LL, Zhang HD. Increased expression of galectin-1 is associated with human oral squamous cell carcinoma development. *Oncol Rep* 2009; **21**: 983–7.
21 Azzimonti B, Pagano M, Mondini M *et al.* Altered patterns of the interferon-inducible gene IFI16 expression in head and neck squamous cell carcinoma: immunohistochemical study including correlation with retinoblastoma protein, human papillomavirus infection and proliferation index. *Histopathology* 2004; **45**: 560–72.
22 Martin-Ezquerra G, Salgado R, Toll A *et al.* Multiple genetic copy number alterations in oral squamous cell carcinoma: study of MYC, TP53, CCDN1, EGFR and ERBB2 status in primary and metastatic tumours. *Br J Dermatol* 2010; **163**: 1028–35.
23 Kawauchi K, Araki K, Tobiume K, Tanaka N. p53 regulates glucose metabolism through an IKK-NF-kappaB pathway and inhibits cell transformation. *Nat Cell Biol* 2008; **10**: 611–8.
24 Takahashi T, Takahashi T, Suzuki H *et al.* The p53 gene is very frequently mutated in small-cell lung cancer with a distinct nucleotide substitution pattern. *Oncogene* 1991; **6**: 1775–8.
25 Fujiuchi N, Aglipay JA, Ohtsuka T *et al.* Requirement of IFI16 for the maximal activation of p53 induced by ionizing radiation. *J Biol Chem* 2004; **279**: 20339–44.
26 Chi LM, Lee CW, Chang KP *et al.* Enhanced interferon signaling pathway in oral cancer revealed by quantitative proteome analysis of microdissected specimens using 16O/18O labeling and integrated two-dimensional LC-ESI-MALDI tandem MS. *Mol Cell Proteomics* 2009; **8**: 1453–74.
27 Chen C, Mendez E, Houck J *et al.* Gene expression profiling identifies genes predictive of oral squamous cell carcinoma. *Cancer Epidemiol Biomarkers Prev* 2008; **17**: 2152–62.
28 Song LL, Alimirah F, Panchanathan R, Xin H, Choubey D. Expression of an IFN-inducible cellular senescence gene, IFI16, is up-regulated by p53. *Mol Cancer Res* 2008; **6**: 1732–41.

Supporting Information

Additional Supporting Information may be found in the online version of this article:

Fig. S1. Genome-wide measurement of DNA copy number alterations in oral squamous cell carcinoma (OSCC).

Fig. S2. IFI16 and AIM2 are upregulated in oral squamous cell carcinoma (OSCC).

Fig. S3. Downregulation of either AIM2 or IFI16 expression decreases the growth rate of HSC4 cells.

Fig. S4. Downregulation of either AIM2 or IFI16 expression increases apoptosis in SAS cells.

Fig. S5. Caspase-1 is not activated in oral squamous cell carcinoma cells.

Fig. S6. Treatment with Bay 11-7082 induced apoptosis in oral squamous cell carcinoma (OSCC) cells.

Table S1. Summary of DNA copy number aberrations in 28 oral squamous cell carcinoma (OSCC) tumors.

Table S2. *p53* status in primary oral squamous cell carcinoma tumors (OSCC) and cell lines.

Data S1. Materials and methods.

Data S2. Additional references in Table S2 and Data S1.

Please note: Wiley-Blackwell are not responsible for the content or functionality of any supporting materials supplied by the authors. Any queries (other than missing material) should be directed to the corresponding author for the article.

doi: 10.1111/j.1349-7006.2012.02211.x

Leukemia (2012) **26,** 1238–1246

www.nature.com/leu

ORIGINAL ARTICLE

Clinical significance of CADM1/TSLC1/IgSF4 expression in adult T-cell leukemia/lymphoma

S Nakahata[1], Y Saito[1], K Marutsuka[2], T Hidaka[3], K Maeda[3,4], K Hatakeyama[5], T Shiraga[1,6], A Goto[1], N Takamatsu[1], Y Asada[5], A Utsunomiya[7], A Okayama[8], Y Kubuki[3], K Shimoda[3], Y Ukai[9], G Kurosawa[9] and K Morishita[1]

Cell adhesion molecule 1 (CADM1/TSLC1) was recently identified as a novel cell surface marker for adult T-cell leukemia/lymphoma (ATLL). In this study, we developed various antibodies as diagnostic tools to identify CADM1-positive ATLL leukemia cells. In flow cytometric analysis, the percentages of $CD4^+CADM1^+$ double-positive cells correlated well with both the percentages of $CD4^+CD25^+$ cells and with abnormal lymphocytes in the peripheral blood of patients with various types of ATLL. Moreover, the degree of $CD4^+CADM1^+$ cells over 1% significantly correlated with the copy number of the human T-lymphotropic virus type 1 (HTLV-1) provirus in the peripheral blood of HTLV-1 carriers and ATLL patients. We also identified a soluble form of CADM1 in the peripheral blood of ATLL patients, and the expression levels of this form were correlated with the levels of soluble interleukin 2 receptor alpha. Moreover, lymphomas derived from ATLL were strongly and specifically stained with a CADM1 antibody. Thus, detection of $CD4^+CADM1^+$ cells in the peripheral blood, measurement of serum levels of soluble CADM1 and immunohistochemical detection of CADM1 in lymphomas would be a useful set of markers for disease progression in ATLL and may aid in both the early diagnosis and measurement of treatment efficacy for ATLL.

Leukemia (2012) **26,** 1238–1246; doi:10.1038/leu.2011.379; published online 6 January 2012

Keywords: CADM1/IgSF4/TSLC1; ATLL

INTRODUCTION

Adult T-cell leukemia/lymphoma (ATLL) results from infection with human T-lymphotropic virus type 1 (HTLV-1).[1,2] Following HTLV-1 infection, 2.1 to 6.6% of HTLV-1 carriers will develop ATLL, and most of the ATLL patients will die within a year.[3] An estimated 10–20 million people worldwide are infected with HTLV-1, and HTLV-1 is endemic in southwestern Japan, the island of Kyushu, Africa, the Caribbean Islands and South America.[4] ATLL cells are mainly derived from activated helper T cells with the $CD3^+$, $CD4^+$, $CD8^-$ and $CD25^+$ (also known as interleukin 2 receptor alpha (IL-2Rα)) cell surface markers.[2] A fraction of ATLL cases have been shown to also express forkhead box P3 (*FOXP3*), which is a master gene for regulatory T cells (T-reg), suggesting that some cases of ATLL may originate from HTLV-1-infected T-reg cells.[5,6] For diagnosis, identification of mono- or oligoclonal provirus integration events by Southern blot analysis is one of the definitive markers for ATLL. In addition to viral integration, ATLL cells with multi-lobulated nuclei (called 'flower cells') have been frequently seen in leukemia cells in the peripheral blood of ATLL patients. Hypercalcemia and high levels of either serum lactate dehydrogenase (LDH) or soluble IL-2Rα (sIL-2Rα) have been found to be unfavorable markers for ATLL; however, these markers are not specific for the diagnosis of ATLL.[7,8]

The developmental steps of ATLL after HTLV-1 infection have remained obscure for 30–40 years. HTLV-1 Tax is thought to be an important viral protein that functions in the maintenance of HTLV-1-infected lymphocytes;[9,10] however, expression of Tax protein was not detected in over 70% of ATLL cases because of genomic deletion and/or DNA methylation.[11–14] Recently, HTLV-1 basic leucine zipper (HBZ) was found to be constitutively expressed in ATLL cells and was shown to interact with JUN and CREB2 to regulate Tax expression.[15,16] HBZ also promotes $CD4^+$ T-cell proliferation in transgenic mice;[16] therefore, HBZ has important roles and functions not only in maintaining the virus life cycle but also in the maintenance of the HTLV-1-infected cells that contribute to disease pathogenesis. Although HBZ is expressed in the majority of ATLL cells, only 5% of HTLV-1 carriers develop ATLL, suggesting that additional factors besides viral infection are required for the development of ATLL.

To identify additional pathogenic factors or novel surface markers for ATLL, we collected gene expression profiles for acute-type ATLL. Using a comprehensive DNA microarray gene expression analysis, we recently demonstrated that cell adhesion molecule 1 (CADM1/TSLC1/IgSF4) is a novel cell surface maker for ATLL.[17] CADM1 was initially isolated as a tumor suppressor for lung cancers by genomic analysis. CADM1 expression is reduced in a variety of cancers by promoter methylation and is associated with poor prognosis and enhanced metastatic potential.[18] By contrast, we identified that high expression of CADM1 has an important role in enhanced cell–cell adhesion to the vascular endothelium, tumor growth and the organ infiltration of ATLL cells.[19]

In this study, we developed various antibodies for CADM1 to be used as diagnostic tools for identifying ATLL leukemia cells.

[1]Division of Tumor and Cellular Biochemistry, Department of Medical Sciences, Faculty of Medicine, University of Miyazaki, Miyazaki, Japan; [2]Pathology Division, University of Miyazaki Hospital, Miyazaki, Japan; [3]Department of Gastroenterology and Hematology, Faculty of Medicine, Miyazaki University, Miyazaki, Japan; [4]Department of Internal Medicine, Miyakonojo National Hospital, Miyazaki, Japan; [5]Department of Pathology, Faculty of Medicine, University of Miyazaki, Miyazaki, Japan; [6]Department of Foods and Human Nutrition, Faculty of Human Life Sciences, Notre Dame Seishin University, Okayama, Japan; [7]Department of Hematology, Imamura Bun-in Hospital, Kagoshima, Japan; [8]Department of Rheumatology, Infectious Diseases and Laboratory Medicine, University of Miyazaki, Miyazaki, Japan and [9]Division of Antibody Project, Institute for Comprehensive Medical Science, Fujita Health University, Aichi, Japan. Correspondence: Professor K Morishita, Division of Tumor and Cellular Biochemistry, Department of Medical Science, Faculty of Medicine, University of Miyazaki, 5200 Kihara, Kiyotake, Miyazaki 889-1692, Japan.
E-mail: kmorishi@med.miyazaki-u.ac.jp
Received 14 April 2011; revised 24 November 2011; accepted 29 November 2011; published online 6 January 2012

We successfully identified ATLL cells in the peripheral blood and in lymphoma samples and detected the soluble form of CADM1 in the peripheral blood of ATLL patients using specific antibodies for CADM1. The CADM1 antibody may therefore represent a useful tool in the diagnosis of ATLL cells.

MATERIALS AND METHODS

Quantification of HTLV-1 proviral load

HTLV-1 proviral DNA load was determined by real-time PCR as previously described.[20] Briefly, genomic DNA from peripheral blood mononuclear cells (PBMCs) was extracted by proteinase K digestion and phenol/chloroform extraction and then subjected to a real-time TaqMan PCR assay using an ABI PRISM 7000 detection system (Perkin Elmer/Applied Biosystems, Forster City, CA, USA) with two sets of primers specific for the *pX* region of the HTLV-1 provirus and the human gene encoding the RNase P enzyme. The primers and the probe for the *RNase P* gene were purchased from Applied Biosystems; those for the *pX* region of the HTLV-1 provirus were described previously.[20] Genomic DNA of normal control PBMCs mixed with a plasmid DNA, which contained almost the whole genome of the HTLV-1 provirus (*Sac*I site of 5′-LTR to *Sac*I site of 3′-LTR), was used as a standard to quantify the proviral DNA copies. The copy number of the plasmid DNA was calculated based on the size and weight of the plasmid DNA, as measured by spectrophotometry. HTLV-1 proviral loads in some of the PBMC samples were measured by the Group of Joint Study on Predisposing Factors of ATL Development (JSPFAD, Japan) as described previously.[21] The amount of HTLV-1 proviral DNA was calculated as the copy number of HTLV-1 per 100 PBMC = ((copy number of *pX*)/(copy number of *RNase P*/2)) × 100.

RESULTS

Frequent expression of surface CADM1/TSLC1 among ATLL-derived cell lines

CADM1/TSLC1/IgSF4 was identified as a novel surface marker on ATLL cells by gene expression profiling using DNA microarray analysis and was found to be frequently expressed in leukemia cells from patients with acute-type ATLL.[17] We first analyzed the CADM1 protein levels in a panel of T-leukemia cell lines using a chicken anti-human CADM1 antibody (MBL, Nagoya, Japan). A 107 kDa band was clearly detected in whole-cell lysates from the KOB, KK1 and S1T cell lines (Figure 1a), which have been reported

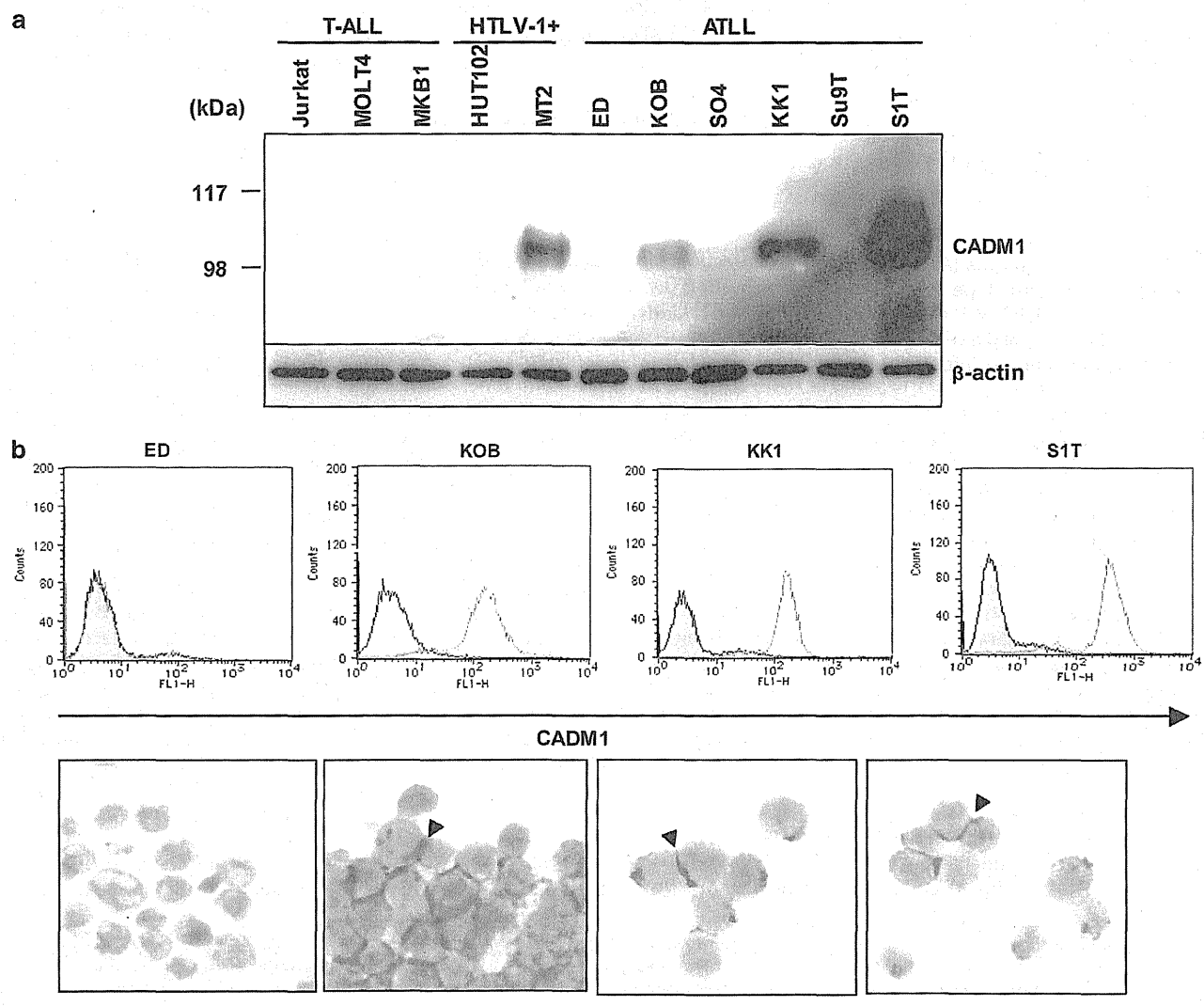

Figure 1. High CADM1 expression in ATLL analyzed by immunoblot, flow cytometry (FMC) and immunohistochemical staining (IHC). (**a**) Immunoblot analysis was performed on a series of T-lymphoid leukemia cell lines (three T-ALL, T-acute lymphoid leukemias; two HTLV-1 +, HTLV-1-infected cell lines; six ATLL, ATLL-derived cell lines) with a chicken anti-human CADM1 antibody. (**b**) A human anti-human CADM1 antibody (051-054), which was established by phage display, was used for FMC and IHC. The anti-CADM1 antibody was visualized by Alexa 488 in FMC and by horseradish peroxidase in IHC.

to express CADM1 according to reverse transcriptase PCR and northern blot analysis.[17] To confirm CADM1 expression on the cell surface of ATLL cells, we examined CADM1 membrane expression by flow cytometry with an Alexa 488-labeled human anti-CADM1 antibody generated by phage-display technology.[22] Four ATLL cell lines were used for flow cytometry: CADM1-negative ED and CADM1-positive KOB, KK1 and S1T cell lines. In all three CADM1-positive cell lines, the fluorescence intensity of CADM1 expression was two logs greater than that of the isotype immunoglobulin G control (Figure 1b, upper panels), while only background levels of fluorescence could be seen in the CADM1-negative ED-ATLL cell line, which had high levels of DNA methylation in the CADM1 promoter region.[17] To evaluate the subcellular distribution of CADM1, immunohistochemical staining was performed on the same cell lines using the anti-CADM1 antibody (Figure 1b, bottom panels). CADM1 was highly concentrated at the cell–cell contact sites in the three CADM1-positive cell lines, and no staining of CADM1 was detected in the ED cell line. These data suggest that CADM1 expression in ATLL cells may promote cell-to-cell contact.

Low levels of CADM1 expression in the T-reg fraction of peripheral lymphocytes

To examine the expression of CADM1 in peripheral blood T-lymphocytes of healthy volunteers, T-reg populations were analyzed for CADM1 expression because $CD4^+CD25^{high}$ T-reg cells are a potential source of ATLL cells.[5,6] Initially, the $CD4^+CD25^+$ cell fraction was separated from PBMCs of a healthy volunteer by the magnetic bead method and stained with an anti-CADM1 antibody. Almost 100% of the S1T-ATLL cell line was strongly stained with the anti-CADM1 antibody; however, 55.8% of the $CD4^+CD25^+$ cells were stained weakly in comparison with the high level of staining of S1T-ATLL cells (Figure 2a). To confirm whether the purified $CD4^+CD25^+$ cells expressing CADM1 were T-reg cells, the sorted $CD4^+CD25^+$ cells were stained for both FoxP3 (a master regulator in the development of T-reg cells) and CADM1. In all, 93% of the $CD4^+CD25^+$ double-positive cells in the peripheral blood were stained by the anti-FoxP3 antibody, while 37% of the cells were stained with both the anti-CADM1 and anti-FoxP3 antibodies (Figure 2b), suggesting that a fraction of the $CD4^+CD25^+FoxP3^+$ T-reg cells weakly expressed CADM1 on their cell surfaces.

We then determined the proportion of $CD4^+CADM1^+$ and $CD4^+CD25^+$ T cells in PBMCs from 10 healthy volunteers after selection with Cy5-labeled CD45 staining. On average, 7.3% of $CD45^+$ cells in PBMCs expressed CD4 and CD25, while only 0.6% of the cell population expressed CD4 and CADM1 (Figure 2c and representative fluorescence-activated cell sorting data are shown in Supplementary Figures 1a and b), indicating that the number of $CD4^+CADM1^+$ cells was significantly lower than the number of $CD4^+CD25^+$ cells in the PBMCs of healthy volunteers. To determine the percentage of $CD4^+CADM1^+$ cells in peripheral lymphocytes of various types of ATLL and HTLV-1 carriers, $CD45^+$ PBMCs from 40 patients diagnosed with various types of ATLL (7 acute-type, 4 lymphoma-type, 6 chronic-type and 23 smoldering-type), 51 HTLV-1 carriers and 10 normal volunteers were analyzed for the surface expression of CD4 and CADM1 by flow cytometry analysis, which was performed by double staining of CD12/CD19, CD3/CD8, CD4/CD25, CD23/CD5, CADM1/CD4, CD20/CD11c, CD16/CD56, CD30/CD7 and κ-chain/λ-chain. The median percentages of $CD4^+CADM1^+$ cells were 73.9% in acute cases, 72.4% in chronic cases (except for a patient with CD4-negative ATLL described below), 5.6% in lymphoma cases, 11.5% in smoldering cases, 4.4% in HTLV-1 carriers and 0.5% in normal volunteers (Figure 2d). In these subjects, the percentages of $CD4^+CD25^+$ cells were significantly correlated with those of $CD4^+CADM1^+$ cells ($R=0.907$, $P<0.0001$) (Figure 2e), suggesting that most of the ATLL cells were $CD4^+CD25^+CADM^+$. However, we also observed a cell surface profile of $CD3^+CD8^-$ (91.3%), $CD25^+CD4^-$ (81.5%) and $CD4^-CADM1^+$ (83.6%) in a case of chronic ATLL, suggesting that the surface markers of the ATLL cells represented $CD4^-CD8^-$ double-negative T lymphocytes that expressed CD25 and CADM1.

CADM1 expression in leukemia cells from ATLL patients and HTLV-1-infected cells from HTLV-1 carriers

To confirm that most of the HTLV-1-infected ATLL cells were indeed in the $CD4^+CADM1^+$ cell fraction, PBMCs from an HTLV-1 carrier and two ATLL patients with chronic or smoldering ATLL were isolated and separated into CADM1-positive and CADM1-negative cell fractions by anti-CADM1 antibody-conjugated magnetic beads. The cell fractions were then analyzed for the expression of CD4 and CADM1 by fluorescence-activated cell sorting analysis (Supplementary Figure 2). In these three patients, 3.4 to 31.4% of PBMCs were positive for CD4 and CADM1. After separation by the magnetic CADM1 antibody, 73.5 to 96.5% of the cells were $CD4^+CADM1^+$. To assess whether these $CD4^+CADM1^+$ cells indeed represented the HTLV-1-infected cell population, the HTLV-1 status was determined by PCR of the proviral DNA with primers against the *HBZ* region of the HTLV-1 genome. As shown in Figure 3a, the HTLV-1 genomic sequence was detected in the three CADM1-positive cell fractions, while weak or no signal was detected in the CADM1-negative cell fractions, indicating that the majority of HTLV-1-positive cells are present in the CADM1-positive cell fractions.

Next, the percentages of $CD4^+CADM1^+$ cells were compared with those of abnormal lymphocytes or with the DNA copy numbers of HTLV-1 in PBMCs of patients with various types of ATLL, which included 6 acute-type, 8 chronic-type and 6 smoldering-type of ATLL, and 20 HTLV-1 carriers (Figures 3b and c). The percentages of $CD4^+CADM1^+$ cells showed a high degree of correlation with those of abnormal lymphocytes ($R=0.791$, $P<0.0001$) and with the HTLV-1 DNA copy numbers ($R=0.677$, $P<0.0001$) in these patient samples. Notably, in two samples from chronic- and smoldering-type ATLL patients, the number of $CD4^+CADM1^+$ cells was less than one-half of the number of HTLV-1 DNA copies (32.0% vs 107.97 copies and 30.0% vs 65.76 copies), which may be due to multiple copies of proviral DNA in the cells. In addition, the percentages of $CD4^+CADM1^+$ cells were correlated with the levels of sIL-2Rα ($R=0.586$, $P<0.0001$) and with the levels of LDH ($R=0.486$, $P=0.0015$) (Figures 3d and e). Consistent with earlier studies, both serum sIL-2Rα and LDH levels were correlated with the HTLV-1 DNA copy numbers ($R=0.705$; $P<0.0001$ and $R=0.44$; $P=0.0045$, respectively) in this study (data not shown).

To further evaluate the diagnostic efficacy of measuring CADM1-positive cells to detect HTLV-1-infected cells, the copy number of the HTLV-1 provirus in PBMCs of carriers was compared with the percentages of $CD4^+CADM1^+$ cells and the serum levels of sIL-2Rα and LDH. The percentage of $CD4^+CADM1^+$ cells showed a significant correlation with the HTLV-1 DNA copy number ($R=0.921$, $P<0.0001$) (Figure 3f), while there was a poor correlation between HTLV-1 copy number and the levels of sIL-2Rα and LDH (data not shown). A correlation between the percentage of $CD4^+CADM1^+$ cells and abnormal lymphocytes was also observed in the HTLV-1 carriers ($R=0.819$, $P<0.0001$), although abnormal lymphocytes and $CD4^+CADM1^+$ cells were very rare in these subjects (Supplementary Figure 3). On the basis of these data, in addition to the determination of copy numbers of HTLV-1 proviral DNA, quantification of $CD4^+CADM1^+$ cell number by flow cytometry may be useful for monitoring the number of HTLV-1-infected cells in the peripheral blood of ATLL patients and HTLV-1 carriers.